Material models for rail pads

Johannes Jacobus Heunis

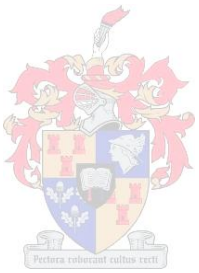

Material models for rail pads

by

Johannes Jacobus Heunis

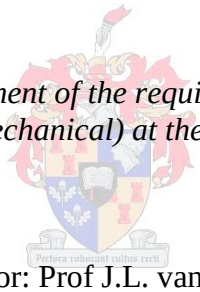

Thesis presented in partial fulfilment of the requirements for the degree Master of Science in Engineering (Mechanical) at the University of Stellenbosch

Supervisor: Prof J.L. van Niekerk

Faculty of Engineering

Department of Mechanical and Mechatronic Engineering

March 2011

Declaration

By submitting this thesis electronically, I declare that the entirety of the work contained therein is my own, original work, that I am the sole author thereof (save to the extent explicitly otherwise stated), that reproduction and publication thereof by Stellenbosch University will not infringe any third party rights and that I have not previously in its entirety or in part submitted it for obtaining any qualification.

Signature: 

J.J. Heunis

Date: 29 November 2010

Copyright © 2010 Stellenbosch University

All rights reserved

Abstract

The vibrations and noise “pollution” that rail vehicles produce have become of particular concern in recent years. More pressure is being placed on operators of trains and trams (especially those operating in urban environments) to reduce their impact on neighbouring infrastructure. This project investigated the infrastructure available for vibration and noise mitigation and generated material models for some of the materials used in these types of rail infrastructure.

The most common type of rail infrastructure used in South Africa is ballasted sleepers. Rail pads are sometimes used to reduce the transmitted vibration of these sleepers; this study focused on the materials used in the manufacture of these pads. Since most of these materials can be described as resilient/viscoelastic, the study of literature regarding these materials is essential within the scope of this project.

Models found in literature were adapted by the addition of a non-linear stiffness element to account for the material behaviour at higher preloads. Three commercially available materials were tested and optimisation algorithms applied to determine their material coefficients (damping and stiffness), focusing on the preload and frequency dependency of these coefficients.

Opsomming

Die vibrasie en geraas “besoedeling” wat spoor voertuie genereer het in die in die afgelope paar jare van kritieke belang geword. Meer druk word op operateurs van treine en trems geplaas (veral die operateurs met operasies in stedelike gebiede) om hulle impak op aangrensende infrastruktuur te verminder. Hierdie projek is dus daarop gemik om te bepaal watter infrastuktuur beskikbaar is vir die vermindering van vibrasie en geraas asook die ontwikkeling van materiaal modellle vir sommige van die materiale wat gebruik word in hierdie tipes van spoor infrastruktuur.

Die mees algemene spoor infrastruktuur wat gebruik word in Suid-Afrika is dwarslêers met ballas. Spoor blokke word soms gebruik om die oordrag van vibrasies te verminder vir hierdie dwarslêers en daarom het hierdie studie fokus geplaas op die materiale wat gebruik word in die vervaardiging van hierdie blokke. Aangesien die meeste van hierdie materiale beskryf kan word as veerkragtig/visco, is ‘n literatuurstudie oor hierdie materiale noodsaaklik binne die bestek van hierdie projek.

Modelle wat gevind is in die literatuur is aangepas deur ‘n nie-lineêre styfheids element by te voeg wat voorsiening maak vir die materiale se gedrag by hoër voorspannings. Drie algemene kommersieël beskikbare materiale is getoets en optimeringsprossesse is toegepas om hulle materiaal koëffisiënte (demping en styfheid) te bepaal met die klem geplaas op die voorspanning en frekwensie afhanklikheid van hierdie koëffisiënte.

Dedicated to my parents and friends for their unwavering support.

Table of Contents

List of Tables

List of Figures

Nomenclature

b	Hysteretic damping coefficient
c	Viscous damping coefficient, Rigidity
c_{eq}	Equivalent viscous damping coefficient
D_e	Insertion loss
E	Error function
E	Young's storage modulus
E_1	Young's storage modulus (real component)
E_2	Loss modulus
$F(X)$	Objective function
F_{calc}	Calculated force
F_{trans}	Transmitted force
F_{max}	Maximum/peak force
F_{meas}	Measured force
f	Driving force
f_c	Damping force
f_k	Spring force
$g(X)$	Inequality constraint
$h(X)$	Equality constraint
K_{eff}	Conventional stiffness
k	Stiffness
k_1, k_2	Stiffness coefficient
m	Mass
n	Number of time samples
N	Number of samples
R	Energy dissipated per cycle (at specific amplitude)
S	Search vector
t	Time
Δt	Time increment

u_1, u_2	Cylinder displacement
v_1, v_2	Cylinder velocity
X	Harmonic response amplitude, Design variable
x_1, x_2	Material displacement
$\dot{x}_1, \dot{x}_2$	Material velocity
α	Velocity-squared damping coefficient
α^*	Search distance
β	Coulomb damping coefficient
ξ	Equivalent viscous damping coefficient
θ	Phase angle
η	Loss factor
ω	Excitation frequency
ω_n	Natural frequency

1 Introduction

The use of trains and trams for urban transport has steadily increased and a recent example of this is the Gautrain rapid rail link project in South Africa. The Gautrain project is a R25-billion (2008) passenger train network in Gauteng Province which will eventually connect Johannesburg, Tshwane (Pretoria) and the OR Tambo International Airport. This system will initially have ten stations and will be South Africa's first modern public rail transport system. The total length of tracks will be approximately 80 km, of which at least 15 km is in tunnels (a first in South Africa).

Increased public and government pressure is being placed on train operators to minimise the vibration and noise generated by their trains. Since vibrations are a main factor in the degradation of the superstructure and rolling stock, an added advantage of these measures is a decrease in maintenance and associated costs.

Damping is a physical phenomenon occurring in all materials to a lesser or greater degree. In the rail environment, damping is introduced to the system by adding resilient or viscoelastic elements to decrease the vibrations transmitted from the rails to the nearby infrastructure. These materials are difficult to model since they introduce non-linearity to the system. The focus of this project was the development of material models for these damping materials.

This chapter gives some background on the causes and physics of railway vibration and noise. The objectives and scope of this project are discussed and the chapter concludes with an overview of the rest of the project and this thesis.

1.1 Railway vibration and noise

There are various methods and materials available to reduce the vibration and noise generated by trains and a number of these methods utilise resilient or viscoelastic materials. These vibrations can be damped at the source (i.e. train or tram), along its transmission path (i.e. rails, sleepers, air etc.) or at the receiver (i.e. buildings). For the purpose of this project, the focus is placed on the interventions that take place along the transmission path. A few of the most common methods of reducing vibration are rail pads, sleeper pads, baseplate pads, embedded rails and resilient sleepers. According to ISO 14837 (2005), softer primary and secondary train suspension, acoustic barriers and smoother wheels and rails are some of the measures that can be implemented to reduce the noise generated by rail vehicles.

According to ISO 14837 (2005), the sources of vibration and noise are as follows:

- Moving loads excitation (a wave moving through the track and supports as the train travels along the track).
- Wheel/rail roughness.
- Parametric excitation (differences in the stiffness due to discrete support and spacing of rolling stock can be considerable when the frequencies coincide with the natural frequencies of the track and supports).
- Wheel/rail defects.
- Discontinuities of track (gaps, joints, dipped rails etc. cause impact forces).
- Steel hardness (variations in hardness).
- Lateral loads (when the vehicle goes around tight curves).
- Mechanical/electrical sources of vibrations (fans from ventilation in tunnels may cause secondary vibrations).

ISO 14837 (2005) states that ground vibrations are mostly carried via surface waves in “normal” railways whereas compression and shear waves are the main mechanism in underground railways.

Most frequencies below 250 Hz are damped by the ground, but under certain conditions, these higher frequencies can be transmitted. The ground may also alter the frequency spectrum and lower frequencies may become more pronounced as the distance that the wave travels increases. Special attention needs to be paid to man-made underground structures and the moisture content of the ground as this could affect the damping/propagation characteristics of the ground considerably.

The most reliable way to evaluate vibration and noise is field measurements. However this method can be costly, time consuming and needs existing infrastructure (track, train etc.) for testing. An easier evaluation method is therefore sought that can be used in the design phase of a new track.

1.2 Objectives and scope

The main objective of this project was the development and implementation of a material model that can be used for the prediction of the vibration generated by rail traffic. Since there are so many different types of track, this project focused on ballasted tracks with rail pads (the most common rail infrastructure in South Africa and also used for the Gautrain). Different damping models were considered and focus was placed on the potential interaction between the materials and the other rail infrastructure affected.

The objectives of the project are summarised below:

- Conduct a literature study to determine typical rail infrastructure and the associated solutions for reducing vibration and noise.
- Conduct a literature study to determine what material models, damping models and mechanical tests exist for viscoelastic materials.
- Test common viscoelastic materials with the aim of characterising their dynamic properties.
- Generate material models and apply an optimisation process to determine the model coefficients with experimental data.

1.3 Thesis overview

The general outline of the project and the outline of each chapter are briefly discussed in the following section.

Chapter 2, the literature study, focuses on rail infrastructure, railway vibration mitigation, viscoelastic material testing, vibration and noise in the rail environment while Chapter 3 places focus on models used for damping. In Chapter 4, the focus is on the testing of materials with the test setup, measurement principle and some test data being discussed. Optimisation results are presented in Chapter 5 with some benchmarking included. Chapter 6, the final chapter, presents conclusions and gives some suggestions for further investigation.

2 Literature Study and Background

The literature study establishes what research has been completed with regard to the testing and modelling of viscoelastic materials while the background lays focus on current rail infrastructure. Various track types are currently in use and with these different track types a range of vibration mitigation solutions can be implemented. Different authors have investigated dynamic models for these track types and found them to be useful tools for the study of vibrations caused by moving trains.

Viscoelastic material properties are difficult to quantify since they exhibit hysteresis and non-linear properties for their force versus displacement characteristics. Due to these complexities, better material models are sought and a lot of testing needs to be conducted on the relevant materials. The main objective of this chapter is therefore to place this project in context and provide background information regarding railway infrastructure.

2.1 Track types

Krüger and Girnau (2007) mentions a number of rail track types for urban and regional rail applications. The main types of track are:

2.1.1 Ballast track

Ballasted tracks are mainly used for regional transport of passengers and goods. It consists of rails and sleepers mounted on a ballast bed. The main advantages of ballasted tracks are their low construction costs and inherent vibration damping. The main disadvantage of ballasted tracks is maintenance related since the ballast may degrade and need replacement or realignment that is both costly as well as time consuming.

2.1.2 Covered track

Covered tracks are mainly used in cities (trams etc.) where space is limited and road or pedestrian traffic may also need to use the area where the track is installed. Only the rails are exposed on the surface and the other infrastructure is covered by a road surface. The main advantages of covered tracks are that track areas can be used by other modes of transport. The main disadvantage of covered tracks is maintenance related, replacement is costly, timely and disruptive to other traffic since the track is embedded in the road surface.

2.1.3 Slab track

Slab tracks are mainly used for high-speed rail tracks, tracks in tunnels, tracks on bridges and tracks which require little maintenance (e.g. covered tracks and green tracks). It consists of rails and/or sleepers mounted or cast into a solid base. The main advantage of slab tracks is that it is almost maintenance free. The main disadvantage of slab tracks is that they are costly and difficult to adapt/change.

2.1.4 Green track

Green tracks are mainly used when rail tracks have to fit in with the environment and to create green spaces. It consists of rails and most of the other infrastructure (e.g. slab track) is covered with vegetation. The main advantages of green tracks are that it is visually appealing, creates a more pleasant urban environment and it may decrease the emitted noise. The main disadvantages of green tracks are that they require regular care and raise additional safety concerns such as fire hazards.

2.2 Vibration mitigation solutions

Since there are a few different railway track types in use, it follows that there would be different solutions to reduce or eliminate the vibrations generated by these track types. The most common solutions are as follows:

2.2.1 Rail pads and rail bearings

The simplest solution to isolate rail track systems is rail pads and rail bearings. As can be seen in Figure 2-1 below, an elastic element is introduced between the rail and sleeper (rail pad) or slab track (rail bearing). This type of intervention can easily be retrofitted to existing systems but is limited toward the vibration isolation it offers. These materials are usually thin (less than 10 mm) to limit the unwanted static deformation of the rail. Rail pads are always subjected to a preload (due to the fastening mechanisms) and this can have a negative influence on their dynamic properties since their dynamic range is decreased.

Figure 2-1: Rail pad and rail bearings

(Elastic solutions for track superstructure, 2002).

2.2.2 Sleeper and baseplate pads

This is a simple solution to isolate rail track systems. As can be seen in Figure 2-2, an elastic element is introduced between the sleeper and ballast (sleeper pad) or baseplate and slab track (baseplate pad). This type of intervention can easily be retrofitted to existing systems and sleeper pads are sometimes incorporated into the design of the sleeper. These materials are usually thicker than rail pads (approximately 20 mm) and in the case of sleeper pads may require extra protection from the ballast stones (the stones have sharp edges which may damage the pads).

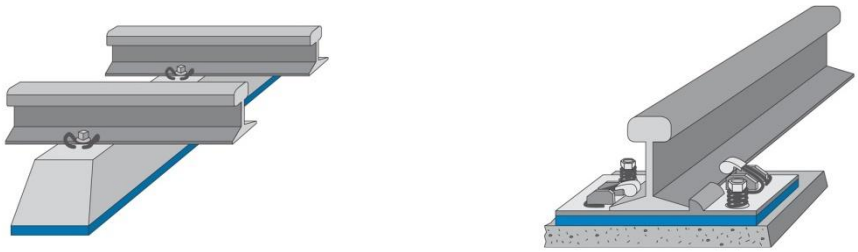

Figure 2-2: Sleeper and baseplate pads

(Elastic solutions for track superstructure, 2002).

2.2.3 Floating trackbeds and ballast mats

This is the most effective solution to isolate rail track systems. As can be seen in Figure 2-3, an elastic element is introduced between the supporting foundation and the ballast (ballast mat) or slab track (base mat). This type of intervention provides a high degree of damping and is typically incorporated into the design of a rail track system from the start. The ballast or slab track act as inertia mass and results in a big static load. To be most effective this system is usually used with side mats and in the case of slab tracks even isolators such as steel springs can be used.

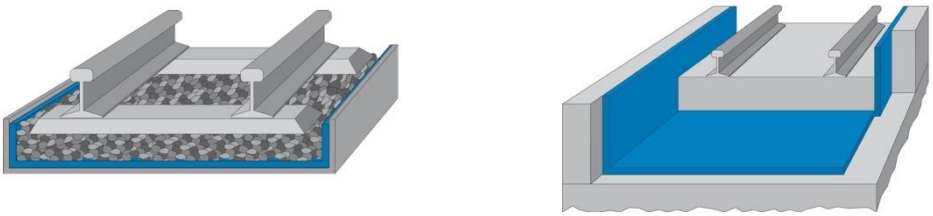

Figure 2-3: Ballast and base mats

(Elastic solutions for track superstructure, 2002).

2.2.4 Embedded rails

This is a specialised solution to isolate rail track systems, it is used exclusively for light rail transport (like trams) where the rail and road infrastructure are shared. As can be seen in Figure 2-4, an elastic filler material is introduced on the sides of the rail and a rail pad encapsulates this assembly. Some manufacturers combine

the rail pad and filler. This type of intervention provides a high degree of damping for re-radiated noise and vibration to the foundations and surrounding environment. As these rails are usually embedded in concrete, the rail pad is designed to bind with the surrounding concrete.

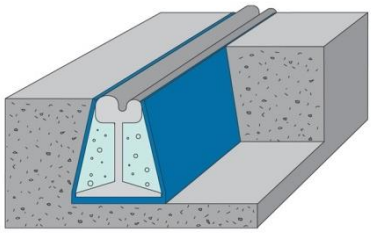

Figure 2-4: Embedded rails (Elastic solutions for track superstructure, 2002).

2.3 Track models

ISO 14837 (2005) provides a detailed checklist to determine/define the relevant parameters to be used for models of the various tracks. The most common models used to model ground-borne vibration and/or noise are parametric models and/or empirical models. The most common models are discussed in more detail below:

2.3.1 Algebraic Models

Algebraic models are parametric models and often simplified, they struggle to simulate soil-structure interaction. Special attention should be placed on the soil models.

2.3.2 Numerical models

Numerical models are parametric models and can be used when sufficient properties of the system are known. Special attention should be paid to the time-step size and element size. Four common numerical methods are given by ISO 14837 (2005):

- Finite element method (FEM) - the system is represented as a mesh and iteration is used to solve continuity functions across the boundaries of elements.
- Finite difference method (FDM) - the system is discretised and differential equations are used to do step-wise calculations in the time domain for the different elements.
- Boundary element method (BEM) – this method is an alternative to FEM and only uses elements on the surface of the model.
- Hybrid models – this method typically uses FEM and FDM to solve source solutions and BEM to solve propagation from source to receiver.

2.3.3 Empirical models

Empirical models are derived from measured data by interpolation or extrapolation. When extrapolating data insertion gains and modulus of transfer functions should be used. Two common empirical methods are given by ISO 14837 (2005):

- Single site models – these models are generated from measurements at a single site and subsequent extrapolations will be made thereafter.
- Multiple site models - these models are generated from a large database of measurements and will try to include variations in all the main parameters.

2.3.4 Semi-empirical models

These models are a combination between empirical and parametric models with one or more empirical component being replaced by analytical equivalents or measurements.

2.4 Track models in literature

Castellani (2000) developed an algebraic model for the vibrations generated by urban rail vehicles on floating slab tracks. Castellani (2000) measured the displacement and acceleration of a floating slab track when a locomotive with seven passenger cars travels over it at 90 km/h and compared the results to a numerical simulation. The numerical simulation exhibited a good correlation to the physical set-up up to about 63 Hz. Castellani (2000) also found that a major shortcoming in his model was a description of elastomeric (resilient) materials with frequency dependent behaviour. These materials show strain rate sensitivity and hysteretic energy dissipation.

Zhai and Cai (1997) generated a numerical model for the dynamic interaction between a rail vehicle and a train track. The different components of the system were modelled as springs, dampers and masses with the ballast being modelled as shear springs and dampers. Wheel/rail interaction was modelled with non-linear Hertzian theory and the equations of motion were solved with Newmark's explicit integration scheme. Experimental validation of the model was done through various field tests and the model showed good correlation with measurements conducted on actual train tracks.

Zhai et al. (2004) focused on the damping mechanisms in the ballast of train tracks. They implemented shear damping and stiffness to model the interaction between the particles. This model was then verified by field testing and found to agree well with the measured results. The calculated resonance frequencies were on average lower than the measured values, 70 to 100 Hz compared to 80 to 110 Hz.

Fiala et al. (2007) developed a numerical model that can be used to predict the vibrations and reradiated sound in buildings due to surface rail traffic. This model accounts for a moving vibration source, dynamic soil structure interaction and

sound propagation through layered ground. The methods used are explained using a numerical example and the model shows good correlation for relatively stiff soil and direct excitation of the foundation.

Fiala et al. (2007) further states that the dominant frequencies with regards to noise is determined by the acoustic resonance of the room, this acoustic resonance is dependent on the wall absorption and room dimensions. It was also found that base isolation is the most effective solution for noise isolation and that the model is dependent on material properties as well as structural details of the buildings.

Karlström et al. (2006) developed an analytical model to predict ground vibrations caused by railways. The main components involved were rails, sleepers, ground and a rectangular embankment which supports sleepers and rails. There are therefore no rail pads or other elastic components involved and focus is placed on modelling the ground vibrations.

Karlström et al. (2006) drew a comparison between two FEM and analytical modelling methods. Analytical methods offer fast computational times and infinite domains but are rather limited towards geometry and non-linear behaviour. FEM (and other discretization) methods overcome the limitations of analytical approaches but has the disadvantages of struggling with infinite domains, long computational times and a small discretized region (it could only deal with 40 m of track).

The results for the model at speeds of 70 km/h and 200 km/h are compared to simplified models and measured data. Their simulations were found to agree almost exactly with measured data at low speeds and showed good correlation with their measured data at high speed. The simplified models were found to show good correlations with the simulation and measured data up to 1 Hz but differs significantly at higher frequencies.

Cox et al. (2006) designed and manufactured a test rig to evaluate slab track structures for specifically underground railways. Their main aim was to develop a test rig that bridges the gap between full scale and bench top tests with regard to the measurement/comparison of the dynamic properties of various fixation systems. The frequencies they mere mostly interested in was between 40 and 120 Hz as these frequencies are most likely to cause disturbances in surrounding buildings.

A major shortcoming of testing in the field was found to be variables such as train speed as well as soil conditions and therefore a test rig could be better suited for comparison purposes on a shorter timeframe. The track was tested for nine different configurations each using different fasteners and/or rail pads. Cox et al. (2006) found the measured natural frequencies to be higher than in physical systems since their test rig does not include an equivalent to the unsprung mass of the rail vehicle.

An "excitation" model was used to extract parameters for the resilient elements in the tests. The values for dynamic stiffness and damping were adjusted so the response of the model mimicked the measured responses for each different resilient material. This method is limited since only a single dynamic stiffness value can be obtained at a specific frequency. The study found that floating slab tracks perform best when fitted with soft rail fasteners especially in the frequency ranges of concern.

Lombaert et al. (2006) developed a three-dimensional numerical model for normal train track systems and high speed (200 km/h plus) trains. This model was validated against various physical systems. Experiments were used to determine the dynamic characteristics of the soil and track, the transfer functions of the soil, the transfer functions of the track-soil and the vibrations of the track as well as the free field. Further experiments were also conducted to verify the numerical model. The rail pads were modelled as continuous spring-damper connections and no attention was given to complex damping characteristics.

The validation of the numerical model showed relatively good agreement for the track-free field transfer functions, but the numerical model overestimated the response at small distances. Their numerical model for the sleeper response and free field vibrations showed good agreement with the measured data although it has a high dependence on soil properties and a high level of uncertainties. It was also found that a better understanding of the train-track interaction is needed and more field testing is needed (in general this article is not applicable to this work since the speeds involved are much higher and the focus is on the soil's transfer properties (vs. the rail pad properties)).

Kaewunruen and Remennikov (2006) conducted a sensitivity analysis to determine the sensitivity of a concrete sleeper to variations in rail pad parameters. Finite element analysis was used and the rail pad stiffness was varied between 0 and $5x10^9$ N/m with a maximum rail stiffness of $100x10^6$ N/m. Their finite element model incorporated sleeper/ballast interaction and the focus of analysis was on in situ mono-block concrete sleepers. The sleepers' changes in natural frequencies and dynamic mode shapes were used as comparison between different rail pads. It was found that rail pad stiffness has a non linear effect on the effective stiffness of the track system and that it mainly affects the first three vibration modes. High effective stiffness can cause changes in the flexural mode shapes of the track.

Lombaert et al. (2006) developed a three-dimensional numerical model for continuous slab track systems. This model was used to determine the effect of various soil, slab and resilient slab mat parameters on the vibration transfer characteristics of the system. The main area of interest was the comparison between normal (un-isolated) slab track and floating slab track systems for different (soft and stiff) soils. It was found that floating slab track systems have pronounced responses at low frequencies and is better suited to applications where the frequencies involved are higher.

Lombaert et al. (2006) also stated that the resonance frequency of the slab track system should be as low as possible for minimum transmissibility. This resonance frequency is generally limited by the maximum allowable static rail deflection, and physical systems can have resonance frequencies as low as 8 to 16 Hz.

Vostroukhov and Metrikine (2003) developed an analytical model for a railway track that is supported by viscous-elastic pads. These pads were modelled according to the Kelvin-Voigt model. The main aim of their model was to determine the elastic drag that a high speed train experiences and they found that the elastic drag is comparable to aerodynamic drag at high velocities.

Nielson and Oscarsson (2004) developed a numerical method for simulating the dynamic train-track interaction. This method separates the track properties into linear (associated with the unloaded track) and non-linear (associated with the dynamic loading) contributions. A moving mass model was then employed for simulation purposes. The dynamic properties of the rail pads was determined in laboratory measurements and quantified with a three parameter state-dependent viscoelastic model. They compared this model to field measurements and found good agreement between the two methods.

Picoux and Le Houédec (2005) developed and validated a numerical model for the vibration generated by trains. The main aim was to model vibrations in the soil and a fairly complex three dimensional model was developed. In situ testing was done to verify this model, these tests made use of optical as well as acceleration measurements. It was difficult to compare numerical and measured data since the excitation frequency was quite difficult to determine, but good agreement was found and the model can be used for further analysis purposes.

2.5 Noise

Heckl et al. (1996) studied the sources of structure-borne sound and vibration caused by rail traffic. They found that the dominant frequencies for noise was in the range of 40 to 100 Hz and are mostly related to the wheel/track resonance. It was also found that most ground vibrations are dominant in the 40 to 80 Hz range, but these vibrations are dependent on the train speed and infrastructure.

They investigated various possible vibration generation mechanisms distinguishing between supersonic motion and accelerated motion. Supersonic motion causes a Mach cone in front of an object when it's moving forward at a speed greater than the wave speed in the medium it is moving. Only bending wave speed in the rails and Rayleigh waves in the ground were considered as they had wave speeds which could be lower than that of the train. It was found that neither of these waves was slow enough to coincide with the speeds that normal passenger trains travel at.

Other major contributors to ground-borne vibration are flat spots in wheels, rail gaps and surface irregularities of the rail or wheel. It was found that a maximum acceleration of 1 m/s^2 can be caused by a train travelling at 144 km/h with an irregularity in one of its wheels. Parametric excitation was also investigated and it was found that stiff rails can solve most of the problems associated with it. It was also found that the wheel-ballast resonance is at about 66 Hz which makes it dependent on train speed (slow trains can more easily excite this frequency).

With further investigation, it was found that the most effective solution to the vibrations involve a highly resilient element and a high dead weight (typical of floating trackbeds and ballast mats). Other solutions include smoother wheels and tracks, stiff rails and various resilient elements along the transmission path of vibrations.

Alvelid and Enelund (2007) developed a special finite element model for the rubber in a steel-rubber-steel sandwich. The type of rubber modelled was "Nitrile" and this type of sandwich is usually used for sound insulation. In general this article is not really applicable to this work since the rubber layers are thin, and therefore stiff. Their model was compared to an ABAQUS finite element model as well as an analytical solution and found to be accurate and efficient.

Different types of track design offer various advantages when considering noise control, Table 2-1 supplies guidelines for comparing different track designs to a ballast bed with wooden sleepers:

Table 2-1: Noise difference for different track types compared to default (Krüger and Girnau, 2007).

Track type	**dB(A) difference**
Ballast bed with concrete sleepers	2 dB(A) increase
Embedded tracks and non-absorbent slab track	5 dB(A) increase
Green track with grass	2 dB(A) reduction

Krüger and Girnau (2007) mentions that recent studies have shown that there is no significant difference between the noise generated by steel, concrete and wooden sleepers. It can be seen that the most efficient track type for controlling noise is green tracks, it is however not always possible to use these types of tracks and other measures include:

- Acoustic barriers in transmission path (maximum reduction of 5 dB(A) for low barriers).
- Soundproof windows in buildings (maximum reduction of up to 45 dB(A)).
- Soft rail fasteners for slab track.
- Absorbent coverings for ballastless tracks (maximum reductions of up to 3 dB(A)).

For frequencies in the measured range (630 Hz to 3,16 kHz), the main source of vibration appears to be the wheels (800 Hz and 1 000 Hz). The main cause of wheel noise is the roughness of the track and since embedded track can pick up a lot of dirt and grit they tend to generate the most noise. For lower frequencies, the structure-borne noise of the sleepers (500 Hz) tends to dominate.

2.6 Vibration and noise from trains

The choice of track, maintenance done and the location of the track have the biggest influence on the vibration and noise generated by rail traffic. A major difficulty with the location of tracks is that it has to be easily accessible to passengers and goods. Being so close to built-up areas creates problems with vibration and noise. The amount and type of space available for a railway also determines the type of track to be used, the main options available are:

- Embedded rails in the road surface.
- Tracks between or alongside the lanes of a road.
- Separate tracks on ground level.
- Aboveground tracks on viaducts or bridges.
- Underground tracks in tunnels.

The spread of noise through air and vibration through soil is mainly determined by two variables:

- "Geometric attenuation", this refers to the distribution of vibration energy over an area and this area increases with distance from source.
- Attenuation of vibrations in the surrounding medium (wind, moisture contents, soil type, surface covering, etc. may all affect the transmission characteristics).

Krüger and Girnau (2007) suggest the following solutions to controlling excessive vibration caused by trains (in order of cost and effectiveness) in standard (slab track or ballast bed with elastic fasteners) tracks:

- Replace rail fasteners with softer or more elastic versions.
- Switch to continuous rail fastening with low vertical stiffness.
- Fit elastic soles below the sleepers.
- Fit elastic mats under the ballast or slab track (light mass-spring system).
- Switch to a heavy mass-spring system, add considerable weight and place whole system on bearings.

Other measures that can be applied to reduce vibration emissions are:

- Reduce the excitation by using smoother running surfaces and/or cleaning the tracks.
- Reduce the stiffness of the rail fasteners.
- Avoid excitations caused by rail bedding by switching to continuously supported rails.
- Increase the sprung track weight.

The vibration-damping effect of different track types can be specified in terms of their "insertion loss" (D_e) and three different formulas are given to calculate it. Insertion loss is an indication towards the weighted sound reduction that a system achieves.

2.7 Vibration and noise field testing

BS 7385 (1990) provides a guide to measuring the vibrations experienced in buildings. Vibrations in buildings are mainly measured for the following purposes:

- Recognition - to determine whether the vibrations experienced is of concern for the integrity of the building.

- Monitoring - to determine what the levels of vibration is with reference to a maximum permitted value.
- Documentation - to determine if the prediction models of vibration in a building is correct and the implemented measures are adequate.
- Diagnosis - to determine what types of mitigation/intervention are required for vibration control in a building.

For the purpose of this study the recognition and documentation of vibrations are of concern since no changes to existing infrastructure was planned.

The duration of an excitation force is of great importance and BS 7385 (1990) specifies the two types of sources as:

- Continuous - the excitation force is acting on the structure for longer than five times the resonance response time.
- Transient - the excitation force is acting on the structure for less than five times the resonance response time.

BS 7385 (1990) classifies vibration responses into two types:

- Deterministic - responses that can be described by explicit mathematical functions.
- Random - responses that have no discernable trend.

The type of building plays an important role in the assessment of vibration, certain buildings (e.g. old buildings) may be more susceptible to damage from vibrations. The following factors are to be taken into account when classifying a building:

- Construction type - eight different types each with two subtypes.
- Foundation type - three different types.
- Soil type - six types.
- Historical/political importance - two different types.

A classification table is provided in BS 7385 (1990) and the acceptable vibration level of a building is dependent on all of the four factors above. Other factors to take into account when measuring vibrations in buildings are:

- Natural frequencies and damping - the fundamental shear frequency of 3 m to 12 m buildings is typically 4 Hz to 15 Hz.
- Building base dimensions - the wavelength of the vibrations plays an important role and building foundations may act as a filter.

When monitoring vibrations, the preferred transducer position is at ground floor level as close as possible to the main load-bearing external wall (where vibrations "enter" the building). If analytical studies are done on vibrations, the transducer position will depend on the modes of deformation and when considering ground-borne sources, transducer placement should be done close to foundations. For the study of shear deformation, transducers should be placed directly on load bearing members and when considering floor motions, transducers should be placed where maximum deflections are expected (usually mid-span).

2.8 Effects of vibration and noise

ISO 14837 (2005) provides an overview of vibrations and the subsequent noise for rail applications. It is necessary to determine if vibration and/or noise caused by a train is within legal limits and various national standards can be consulted. Table 2-2 below gives guidance towards the frequencies of concern with vibrations and noise:

Table 2-2: Frequencies of concern.

Vibration type	Frequency range	Reference
Perceivable ground-borne vibration	1 Hz to 80 Hz	ISO 14837 (2005)
Perceivable ground-borne noise	16 Hz to 250 Hz	ISO 14837 (2005)
Perceivable airborne noise	600 Hz to 3 kHz	ISO 14837 (2005)
Effects on buildings	1 Hz to 500 Hz	ISO 14837 (2005)
Effects on sensitive equipment	<1 Hz to 200 Hz	ISO 14837 (2005)
Airborne noise	600 Hz to 3 kHz	ISO 14837 (2005)
Perceivable building vibration	3 Hz to 80 Hz	ISO 14837(2005)
Ground-borne (secondary) noise	30 Hz to 160 Hz	ISO 14837(2005)
Damage to buildings	1 Hz to 150 Hz	BS 7385 (1990)
Natural sources (e.g. earthquakes)	0,1 Hz to 30 Hz	BS 7385 (1990)
Wind loading	0,1 Hz to 2 Hz	BS 7385 (1990)
Ballast resonance	66 Hz	Heckl et al. (1996)
Ground vibrations	40 to 80 Hz	Heckl et al. (1996)

2.8.1 Perception of ground-borne vibration

Ground-borne vibration is caused by irregularities on wheels and rails as well as the discrete nature of support provided by sleepers. To minimize this excitation, the distances between wheels should be designed not to be multiples of the support spacing (and vice versa). Rails and/or wheels that are correctly maintained, installed and designed also helps to minimize this vibration. Ground-borne vibration transmitted to buildings can have the following effects on humans:

- Annoyance.
- Discomfort.
- Activity disturbance.
- Negative effects on health (extreme cases).

2.8.2 Perception of ground-borne noise

Ground-borne noise is a result of vibrations and therefore the same forms of excitation exist. To minimize this excitation, the same measures are applicable as with ground-borne vibration and normal noise-protection measures are not successful at minimizing these vibrations. Ground-borne noise is usually caused by the secondary vibration of building surfaces and can have the following effects on humans:

- Annoyance.
- Activity disturbance.
- Sleep disturbance.

2.8.3 Perception of airborne noise

Structure-borne noise is mainly caused by the vibrations resulting from steel wheels rolling on steel tracks. This noise is linked to the roughness of the track and less noise is emitted by rails and/or wheels that is properly maintained and designed. Airborne noise is usually the most noticeable form of noise and a number of regulations exist that stipulates the maximum allowable noise levels.

2.8.4 Effects on buildings

Ground-borne vibration can cause damage to buildings in extreme cases but the levels required for damage are more than 10 times larger than human perception (most humans would therefore vacate the building before damage occurs).

2.8.5 Effects on sensitive equipment and tasks

Ground-borne vibration can hamper the operation of sensitive equipment (e.g. computer hard drives and relays) but in general the shocks and vibration from their normal service environment (e.g. door slams) has far higher levels of vibration. Vibration-sensitive equipment usually has detailed specifications towards the maximum allowable vibration and special measures might be needed to protect this equipment from excessive vibration.

2.9 Viscoelastic material tests

The most general laboratory test standard for determining the vibration and acoustic transfer properties of resilient materials is ISO 10846 (1997). ISO 10846 (1997) can be used to determine the transmission of low frequency (1 Hz to 80 Hz) vibrations by these elements but makes a number of assumptions. It assumes linearity of the behaviour of the isolator and that all contact surfaces can be considered to be point contacts. According to ISO 10846 (1997) there are three different test methods (direct, indirect and driving point methods) that can be used to test the properties of resilient elements used for support.

Carrascal et al. (2007) tested rail pads to determine the degradation experienced by these pads. The pads were fatigue tested at various operating temperatures, humidity and loads for up to 200 000 cycles to determine how their dynamic properties changes over time. They evaluated this deterioration in terms of the dissipated energy per cycle and the change in dynamic stiffness. It was found that the major source of degradation is humidity and in the worst case a stiffness increase of 12% was found. Dynamic stiffness tests were conducted for 1 000 cycles at 5 Hz at different temperatures. To evaluate the change in static stiffness, the pads were tested at five different conditions for 200 000 cycles at 5 Hz with loads between 18 kN and 93 kN.

Carrascal et al. (2007) also conducted conventional fatigue tests for 2×10^6 cycles at room temperature at the same load variation as the dynamic stiffness tests. It was observed that the greatest variation in energy dissipation and dynamic stiffness took place during the first 200 000 cycles and becomes less pronounced thereafter. The dynamic stiffness increased by 18,5% and the energy dissipation decreased by 41,6%. It was also noted that the temperature of the pad increased by 7° C during these fatigue tests.

Dall'Asta (2006) et al. tested high damping rubber (HDR) with the aim of obtaining accurate material properties and to develop a non-linear viscoelastic damage model for cyclic loads. HDR consists of natural rubber with black carbon filler added to increase damping and strength. This filler also adds undesirable material properties. HDR dampers are promising energy dissipation devices, they permit energy dissipation even for small events (wind or minor earthquakes) and have no "memory". Viscoelastic and viscous dampers have similar properties, but their energy dissipation capacity is sensitive to strain-rates.

Dall'Asta (2006) et al. subjected various materials to tests at various frequencies and amplitudes. Their stiffness and dissipating properties were classified by using three parameters (K_{eff}, R, ξ). Where K_{eff} is the conventional stiffness, R gives information about the energy dissipated per cycle (at a specific amplitude) and ξ is the equivalent viscous damping coefficient. Over a test period of three years, the values of K_{eff} , R and ξ reduced by 22%, 58% and 15% respectively. It was also found that the stiffness (K_{eff}) decreases and R increases with increasing amplitude. The stiffness and energy dissipating properties show major increases when the strain rate is higher than 1 Hz. An analytical model was then developed for use in seismic applications.

Guigou-Carter et al. (2006) tested rail pads and resilient sleeper pads to determine their dynamic stiffness. Their tests were conducted by using the direct method and the setup was tested with various combined horizontal and vertical pre-loads. An analytical model for the track system was then developed. For this model, the damping of each component was modelled as hysteretic damping. It was found that the resonance frequency decreases when the unsprung mass of the train increases and/or the dynamic stiffness of the sleeper pad are decreased. For their model, there was a decrease in vibrations above the resonance frequency and they found that the model could be used to make more informed choices for rail pads.

As previously mentioned, Guigou-Carter et al. (2006) used the direct test method. They used two different static load set-ups during testing, the one setup applied 40 kN vertically and 10 kN horizontally while the other setup applied 64 kN vertically and 5 kN horizontally. It was found that the test rig could only be validated for excitation frequencies below 50 Hz (testing was done at 8 Hz, 16 Hz and 31,5 Hz) since the generated force correction became pronounced at higher frequencies. For an excitation frequency of 8 Hz, the dynamic stiffness increased by 12% for both load cases. For the higher frequencies, the dynamic stiffness increased by more than 20% for the vertical static load of 40 kN and an increase of up to 20% was found for the 64 kN vertical static load. It was found that the dynamic stiffness increased with increasing static loads, as the model predicted.

Maes et al. (2006) tested rail pads and experimentally determined values for the stiffness and damping values (by using a loss factor). Their tests were conducted by using the direct method and they tested in the 20 to 2 500 Hz frequency range with variable pre-loads and three different materials. The materials they studied were all available rail pads, these are EVA (the reference pad), DPHI (polyurethane and cork rubber pad) and SRP (resin-bonded rubber pad). They also developed a material model that can be used in a non-linear numerical track model.

Maes et al. (2006) noted that there are three common ways of modelling the dynamic behaviour of rail pads:

- A spring and viscous dashpot in parallel (Kelvin-Voigt model) - easy to implement but limited in applications.
- A model with structural damping and a loss factor - consistent with behaviour of rubber etc. (but limited to a single frequency).
- A model with three parameters (Poynting-Thompson or relaxation model) - some advantages but difficult to reliably obtain the parameters.

It was found that finding numerical material models by fitting curves to the experimental data from in situ (onsite) tests has certain shortcomings. These measurements are mostly applicable to a particular measured track and are rarely able to take into account the non-linear stiffness of the pads. Laboratory measurements are therefore necessary to obtain more accurate data.

Maes et al. (2006) made use of the direct method for testing rail pads since small specimens (25 mm x 30 mm) were tested and the loads used were relatively small. Rail pads were tested at preloads of 375, 500, 625, 750 and 1 000 N. These loads are equivalent to loads of 15, 20, 25, 30 and 40 kN in rail applications with the first two loads being comparable to the average preloads of rail fixation systems. Dynamic transfer stiffness and loss factors were then calculated with the guidelines in ISO 10846 (1997) and the results were presented for a 500 N preload. It was found that the dynamic stiffness of the pads increase with frequency (pronounced above 2 000 Hz) and preload.

The EVA pad is the stiffest and the most frequency dependent, while that of the DHPI and SRP pads had similar frequency dependent behaviour. The behaviour observed in the rail pads was similar to at least two other independent reports, keeping in mind that different sizes and materials were used. Results for the loss factor were similar, it also increases with frequency but seems to be independent of the preload. It was found that the DHPI pad had the highest loss factor and the loss factor of the EVA pad didn't show the same trend as the other two (possibly because it is stiffer).

Finally, Maes et al. (2006) used a modified Poynting-Thompson model for their material model. The dynamic stiffness of the model shows good correlation with the measured results up to 2 000 Hz. Above 2 000 Hz, this model cannot keep up with the increase in dynamic stiffness. Their model of the dynamic damping shows little correlation to the measured data.

Lin et al. (2005) developed a new test method to determine the frequency dependent behaviour of viscoelastic materials using an impact test. The measured frequency response function and a least squares polynomial curve fitting of test data were used to generate a model for the dynamic stiffness and damping of the material, using a hysteretic damping model. Their test setup made use of accelerometers and a modal hammer. A fast Fourier transform (FFT) of the system response was then analysed to determine the stiffness and damping values of the material.

It was found that only a region (100 to 300 Hz) of the calculated damping coefficients could be used for the least squares evaluation since low frequency rocking motions and noise on the measured signals were present in the obtained data. Frequency dependent functions for the damping coefficients were found and it was assumed that this function is linear in the relevant frequency range. This function had a maximum error of 10% within the specified frequency range. The stiffness was calculated in three different frequency ranges: below resonance (50 to 135 Hz), within the resonance band (135 to 183 Hz) and above resonance (183 to 600 Hz).

To verify the models obtained, the direct method was used and it was found the stiffness values shows a good correlation below 300 Hz. Above 300 Hz, significant deviations were found and the damping was found to show good correlations below 250 Hz. It was also found that the effects of static preload can be taken into account by adjusting the mass and the amplitude of the impact force.

Lapčík et al. (2001) tested rail pads to determine their dynamic stiffness. Their tests were conducted according to the German DB-TL 918.071 standard and they tested in the 10 to 100 Hz (at 2 Hz intervals) frequency range with varying static pre-loads (7,5, 15 and 25 kN). They observed an increase in dynamic stiffness with frequency and/or static-preload.

It was observed that the materials were more compliant at frequencies below 40 Hz and that the dynamic stiffness is dependent on the amplitude of the vibrations. Decreasing the amplitude tenfold led to maximum decreases of 16,2%, 15,5% and 13,5% for the dynamic stiffness with preloads of 0,03, 0,06 and 0,1 MPa respectively. These changes are relatively small and the amplitude dependence of the dynamic stiffness is weak.

The most relevant tests and test parameters found in literature are summarised in Table 2-3 below:

Table 2-3: Summary of viscoelastic testing.

Test type	Excitation frequencies	Load/Preload	Reference
Direct method (ISO 10846 (1997))	8, 16 and 31,5 Hz	40 kN (V*) 10 kN (H*), 64 kN (V*) 5 kN (H*)	Guigou-Carter et al. (2006)
Direct method (ISO 10846 (1997))	20 to 2 500 Hz	15 kN, 20 kN, 25 kN, 30 kN, 40 kN	Maes et al. (2006)
DB-TL 918.071	10 to 1 000 Hz	7,5 kN, 15 kN, 25 kN	Lapčík et al. (2001)

* V - vertical , H - horizontal

Nakra (1998) discussed some of the commercial uses of viscoelastic materials with the focus on vibration control. The two basic forms of energy dissipation are direct and shear strains in the viscoelastic material. Non linearity of the material can be characterized by a loss factor (η), which is the ratio of energy dissipated to energy stored in the material.

If a harmonic stress is applied to a viscoelastic material, the stress in the material tends to lag behind the input by an angle θ. Another difficulty with quantifying viscoelastic materials is the fact that they exhibit different mechanical properties for direct and shear strain, these properties are also dependent on strain rate,

frequency and temperature. Nakra (1998) also discusses methods to take all these factors into account by using fractional calculus.

Remillat (2007) investigated the damping properties of composite materials, especially polymers filled with elastic particles. The approach followed was self-consistent homogenisation and the elastic-viscoelastic correspondence principle was also used. Remillat (2007) used a composite sphere model to include the different mechanical properties of the different materials and the outcome was to optimise the damping of these composites.

Vriend and Kren (2004) investigated an alternate method for quantifying the mechanical properties of viscoelastic materials. This method is called the dynamic indentation method and the Kelvin-Voigt damping model is used to describe the material behaviour. Hardness tests of the material are used to estimate the various properties of materials and the process is similar to the Shore hardness measurement which is already widely used. Traditionally static indentation was used to determine the material properties but with viscoelastic materials the material properties are velocity dependent so a dynamic method is more appropriate. The model generated by Vriend and Kren (2004) is similar to the Kelvin-Voigt model and makes use of the measured logarithmic decrement to determine the rigidity (c) and the viscosity of the material. During testing, it was found that there is a phase shift and residual deformation in the material. The experimental data also showed good correlation for low hardness rubbers without significant creep and can therefore be used to reliably model the damping.

The results/conclusions of previous studies are summarised in Table 2-4 below:

Table 2-4: Results/conclusions found in literature.

Observation	Reference
Stiffness decreases due to fatigue	Dall'Asta (2006)
Dynamic stiffness decreases as humidity increase	Carrascal et al. (2007)
Dynamic stiffness increases due to fatigue	Carrascal et al. (2007)
Dynamic stiffness increases with increasing strain rate (frequency)	Dall'Asta (2006), Maes et al. (2006), Lapčík et al. (2001)
Dynamic stiffness increases with increasing static load	Guigou-Carter et al. (2006)
Dynamic stiffness increases with an increase of preload	Maes et al. (2006), Lapčík et al. (2001)
Dynamic stiffness decreases with decreasing load amplitude	Lapčík et al. (2001)
Energy dissipation decreases as a result of fatigue	Carrascal et al. (2007), Dall'Asta (2006)
Energy dissipation increases when strain rate increases	Dall'Asta (2006)
Equivalent viscous damping decreases as a result of fatigue	Dall'Asta (2006)
Loss factor increases with increasing strain rate	Maes et al. (2006)
Loss factor appears to be independent of preload	Maes et al. (2006)
Resonance frequency decreases with an increase in load and/or decrease in dynamic stiffness	Guigou-Carter et al. (2006)

Macioce (2003) explained methods for quantifying the level of viscoelastic damping in materials. Viscoelastic damping is proportional to the strain and independent of the rate, and can be expressed as follows:

$$E = E_1 + iE_2 = E_1(1 + i\eta) \qquad (2.1)$$

where E_1 is Young's storage modulus, E_2 is the loss modulus and η is the loss factor.

The various methods used were the half-power bandwidth (or 3 dB) method, the amplification factor method, the logarithmic decrement method and the hysteresis loop method. The various methods can be compared for low levels of damping where linear behaviour can still be expected.

2.10 General damping

Bandstra (1983) compared non-linear damping models with their viscous equivalents by using the energy dissipated per cycle as measure. Viscous, velocity squared, Coulomb, displacement squared and solid (hysteretic) damping models were studied and forced as well as transient vibrations applied. Bandstra (1983) found that for forced vibrations, these viscous equivalents underestimate the energy dissipated per cycle as well as the steady state amplitude. When considering transient vibrations, these viscous equivalents show different decay shapes (for Coulomb, displacement squared and solid damping) and times. In general the damped natural frequencies were different using viscous equivalents but the differences were considered insignificant.

Bandstra (1983) found that the equivalent viscous damping method can be used for "fairly accurate" predictions as long as the damping is below 10%. The frequencies at which this method can be implemented is critical, in general this technique is not suited for excitation frequencies close to the natural frequency. Finally, if this method is to be implemented accurately, the actual energy dissipation of the non-linear model has to be known.

Adhikari and Woodhouse (2001) developed a general damping model. This model can be used for both viscous and non-viscous damping and is restricted to linear systems with light damping. Their model takes energy dissipation of a system into account and uses complex experimental data to obtain the parameters for a "relaxation function". A non-viscous damping model is used with convolution integrals over kernel functions. These convolution integrals enable the damping model to depend on the time-history. The kernel function (also called the "relaxation function") is an exponential model which is fitted to measured data.

Numerical experiments were conducted with various damping models and parameters. The model was shown to predict the damping accurately and the transfer functions obtained from the model also agree with the exact transfer functions of the system. This is a promising model, although it could be too complicated.

Adhikari and Woodhouse (2001) explained how it can be determined whether a system has viscous or non-viscous damping. The method for quantifying viscous damping is the half-power bandwidth method and the method for quantifying non-viscous damping is iterative.

Woodhouse (1998) investigated linear damping models with emphasis on structural vibration. Two different models were investigated, the dissipation-matrix and general linear model. To simplify the analysis, small damping was assumed and simple expressions for the damped natural frequencies, complex mode shapes and transfer functions were found.
The different damping mechanisms for structural damping can be divided in three different classes:

- Distributed energy dissipation throughout the bulk material ("material damping").
- Energy dissipation through the junctions or interfaces between the parts of the structure ("boundary damping").
- Energy dissipation through a fluid in contact with the structure.

A simple numerical model of a two-degree-of-freedom system was used as an example for the method and this model provides accurate results over a wide range of values for the different parameters. Woodhouse (1998) also found that it is difficult to determine the appropriate damping model for a structure since it is frequency dependent.

Maia et al. (1998) developed a damping model for materials whose behaviour cannot be modelled accurately by the current viscous or hysteretic models (such as materials with a complex Young's modulus). They used the theory of fractional derivatives to develop a complicated model.

2.11 Conclusion

This chapter provides background to the causes, effects and physics of railway vibration. Previous work done in this field was studied and various principles will be applied with regard to testing and modelling of these materials.

3 Damping Models

This chapter documents the different damping models found in literature. It begins by examining general damping models and progresses to more complex relaxation models.

3.1 General damping models

Several different models exist to represent the damping characteristics of a system. To compare the different damping models to the well known viscous damping model, a simple single degree of freedom system with a non-linear spring was used as shown in Figure 3-1 below.

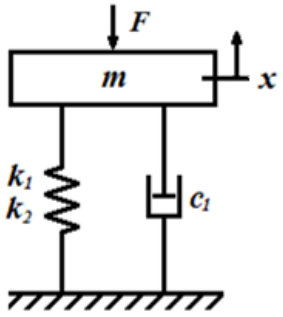

Figure 3-1: Single degree of freedom system diagram.

The transmitted force ($F_{trans}(t)$) of a material under a load can be described as follows:

$$F_{trans}(t) = f_k + f_c \tag{3.1}$$

where f_k is the spring force and f_c is the damping force.

Since the materials showed highly non-linear behaviour, the spring force was calculated as follows:

$$f_k = k_1 x^3 + k_2 x \tag{3.2}$$

where k_1 and k_2 are the stiffness coefficients and x is the displacement.

3.1.1 Viscous damping

$$f_c = c\dot{x}(t) \tag{3.3}$$

According to Inman (2001) this is the "classic" damping model and all the other models were compared to it in our analysis by using the equivalent viscous damping approach. The model is linear with the velocity and is therefore easy and convenient to use. This type of damping can mainly be attributed to laminar hydraulic flow through an orifice as found in automotive shock absorbers.

3.1.2 Velocity Squared damping

$$f_c = \alpha \operatorname{sgn}\left(\dot{x}(t)\right)\dot{x}(t)^2 \tag{3.4}$$

According to Inman (2001) this is a damping model usually associated with aerodynamic drag. To compare it to viscous damping, the damping coefficient (α) can be calculated from:

$$\alpha(\omega) = \frac{3\pi c_{eq}}{8\omega F} \tag{3.5}$$

where ω is the driving force frequency and F is the amplitude of the driving force.

Note the dependency of the calculated damping coefficient on the input frequency (ω), therefore this coefficient can only be used for steady state analysis. This type of damping can mainly be attributed to aerodynamic drag as found in an object vibrating in air.

3.1.3 Hysteretic Damping

$$f_c = b \operatorname{sgn}\left(\dot{x}(t)\right)\left|x(t)\right| \tag{3.6}$$

According to Inman (2001) this is a damping model usually associated with viscoelastic materials. To compare it to viscous damping, the damping coefficient (b) must be:

$$b(\omega) = \frac{\pi\omega c_{eq}}{2} \tag{3.7}$$

where ω is the driving force frequency.

Note the dependency of the calculated damping coefficient on the input frequency (ω), therefore this coefficient can only be used for steady state analysis. This type of damping can mainly be attributed to internal friction energy loss as found in a rubber mount.

3.1.4 Coulomb Damping

$$f_c(t) = \beta \operatorname{sgn}\left(\dot{x}(t)\right) \tag{3.8}$$

According to Inman (2001) this is a damping model usually associated with friction. To compare it to viscous damping, the damping coefficient (β) is calculated as:

$$\beta(\omega) = \frac{\pi \omega c_{eq}}{4} \tag{3.9}$$

where ω is the driving force frequency and β is the amplitude of the driving force.

Note the dependency of the calculated damping coefficient on the input frequency (ω), therefore this coefficient can only be used for steady state analysis. This type of damping can mainly be attributed to friction between two objects as found in disk brakes.

3.1.5 Comparison between the various damping models

To compare the viscous damping model with other damping models, a sinusoidal displacement and velocity were generated (the offset, frequency and amplitude of this input could be changed). The spring and damping force of each model was then calculated and the various damping forces were normalised as follows:

$$f_c = \frac{f_c}{\max(f_c)} \tag{3.10}$$

The spring and damping forces were then added and the corresponding transmitted force was examined. The stiffnesses (k_1 and k_2) used were $0{,}35 \times 10^{12}$ N/m^3 and $0{,}35 \times 10^{6}$ N/m respectively. Since the damping forces were normalised,

their respective values are irrelevant. The displacement (in mm) and velocity (in mm/s) inputs used were as follows:

$$x(t) = 2 + 0{,}9\sin(16\pi t) \tag{3.11}$$

$$\dot{x}(t) = 14{,}4\pi\cos(16\pi t) \tag{3.12}$$

As can be seen in Figure 3-2 below, the various damping models differ considerably in their force-displacement characteristics. The viscous and velocity squared models provide the most accurate representation of the materials tested without introducing the unwanted non-linearity that can be observed in the hysteretic and Coulomb models. As it is the easiest to implement, the viscous model was chosen for further work.

The various damping models also have different frequency dependencies; the viscous model increases linearly with frequency and the velocity squared model increases quadratically with frequency. On the other hand, the hysteretic and Coulomb damping models have no frequency dependency.

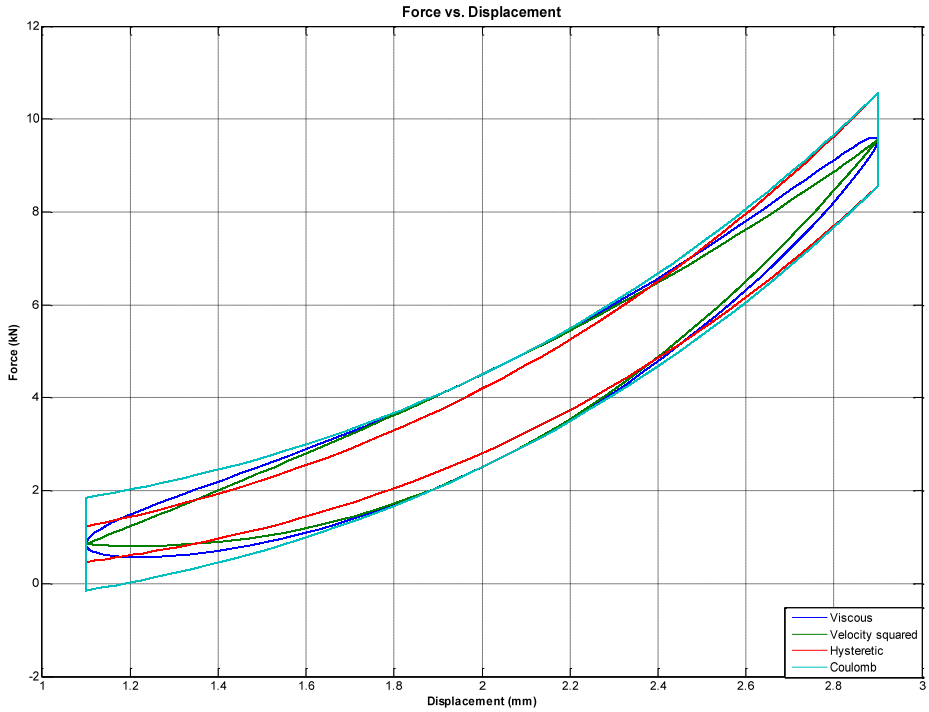

Figure 3-2: Various damping models.

3.2 *Isolator damping models*

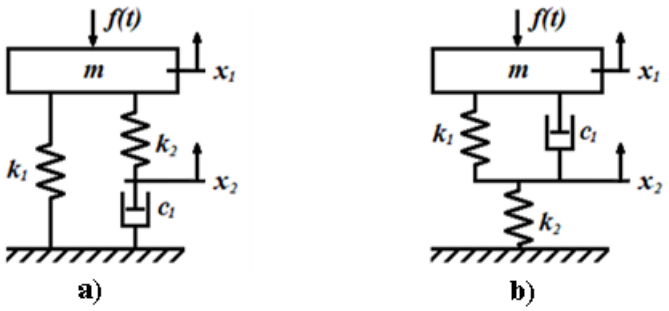

Figure 3-3: Isolator damping models.

The models shown in Figure 3-3 are used to represent systems with a strong frequency dependency. The model on the left (a) is also known as the Relaxation model and the model on the right (b) is known as the Creep model. Maes et al. (2006) showed that the Relaxation model can be used with great success to model the dynamic stiffness of elastic pads up to frequencies of 2 000 Hz but cannot provide accurate modelling of the dynamic damping. The transmitted force ($F_{trans}(t)$) and relative velocity ($\dot{x}_2$) of the Relaxation model under a load can be described as follows:

$$F_{trans} = k_1 x_1 + k_2 \left(x_1 - x_2 \right) = k_1 x_1 + c_1 \dot{x}_2 \tag{3.13}$$

$$\dot{x}_2 = \frac{k_2}{c_1} \left(x_1 - x_2 \right) \tag{3.14}$$

The transmitted force ($F_{trans}(t)$) and relative velocity ($\dot{x}_2$) of the Creep model under a load can be described as follows:

$$F_{trans} = k_1 \left(x_1 - x_2 \right) + c_1 \left(\dot{x}_1 - \dot{x}_2 \right) = k_2 x_2 \tag{3.15}$$

$$\dot{x}_2 = \frac{1}{c_1} \left[k_1 \left(x_1 - x_2 \right) - k_2 x_2 + c_1 \dot{x}_1 \right] \tag{3.16}$$

3.3 Conclusion

This chapter provides background to the different available damping models. It was found that the Viscous damping model is the easiest to implement and that Isolator damping models show great promise in the modelling of viscoelastic materials. Elements of both these models will be implemented in further work.

4 Material Testing

This chapter documents the material testing that was done as part of this study. It starts off with an explanation of the test setup, then examines the different materials that were tested and finishes off with a discussion of sample results.

4.1 Test setup

The test setup is similar to the setup described in ISO 10846 (1997) as the direct method. A MTS load frame and hydraulic cylinder were used for dynamic excitation, and the displacement control of the hydraulic cylinder was done with a standalone MTS 407 Controller. Displacement feedback was achieved using a displacement transducer incorporated into the hydraulic cylinder. During testing, displacement and force measurements were stored with a separate data acquisition system connected to a laptop computer.

The MTS 407 controller (see Figure 4-1 below) is a modern digital PID (proportional–integral–derivative) controller with the functionality and ease of use required for this specific application. This controller includes alternating current (AC) and direct current (DC) conditioning for transducers, has a built in function generator (used during the testing) and can accept external command signals. All the functions of the controller are accessed via a built-in front end interface and output signals can be read and recorded with two BNC connections.

The load frame has structural resonances above 34 Hz and the maximum load rating is in the order of 20 kN. These parameters limit the excitation frequency and the size of the material samples.

Figure 4-1: 407 Controller (Model 407 Controller Product Manual, 2006).

4.2 Measurement equipment

Since the hydraulic cylinder's internal displacement transducer is not accurate enough, displacement was measured using an HBM WA 20 mm displacement transducer to obtain a better resolution. This displacement transducer was calibrated before use with gauge blocks and a recently calibrated HBM S9 20 kN load cell was used for load measurements. In each case, 4 seconds of data was captured at a sampling rate of 1 200 Hz.

Data was acquired with a HBM QuantumX bridge amplifier and data acquisition system connected to a laptop computer. For a typical setup and a detailed list of equipment, see Figure 4-2 and Table 4-1 below:

Table 4-1: Measurement equipment.

Equipment	Detail	Serial Number
Displacement transducer	HBM WA 20 mm	052310184
Force transducer	HBM S9 20 kN	220409A
Bridge amplifier	HBM QuantumX	338515
Servo controller	MTS 407	US1.35268.SPC-40
Load frame	MTS 312.31	170

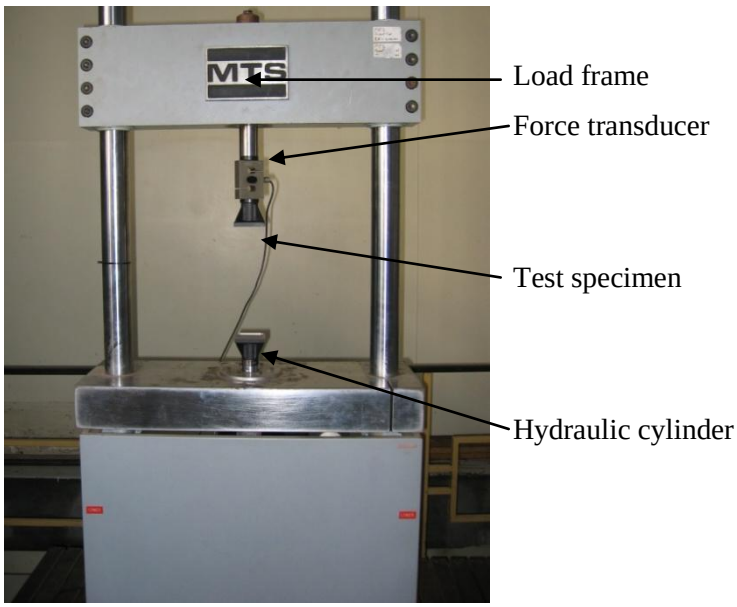

Figure 4-2: General view of test setup.

4.3 Test procedure

The main problem with testing these viscoelastic materials was to determine the loads to which they would typically be subjected. Since the MTS 407 controller was set up for displacement control, preload displacement was set and a sinusoidal displacement was applied around this set point. Forces were applied in only one axis with excitation frequencies of 4, 8 and 16 Hz being used. These frequencies were chosen by using the study of Guigou-Carter et al. (2006) and the system limitations as a guideline.

4.4 Materials

Test samples 10 mm thick and approximately 70 mm x 70 mm in size with mechanical properties suited for rail applications were chosen for testing. The mechanical properties listed in Table 4-2 were supplied by CDM and used as guidelines for the testing.

Table 4-2: Materials and selected mechanical properties (CDM-Solids, 2006).

Name	Static Load Range [MPa]	Static Young's Modulus, E [N/mm^2]
CDM-17	0,5 to 1	8,5 to 12
CDM-45	0,05 to 0,6	3 to 5
CDM-46	0,1 to 0,9	4 to 8

The test specimens are made of various materials and components. In Table 4-3 below, some more information on the composition and range of the materials tested are listed.

Table 4-3: Materials and their composition.

Name	Range	Material
CDM-17	Resin-bonded cork rubber	Cork and rubber
CDM-45, CDM-46	Resin-bonded rubber	Granulated rubber

For more detailed specifications regarding the materials, please refer to Appendix A.

4.5 Sample results

The measured data can be presented as time versus force or displacement or as force versus displacement. The data from a typical measurement is shown in the

figures below. The material tested was CDM-46; it was tested at 8 Hz excitations with excitation displacements of 0,51 ± 0,5, 1,01 ± 0,52 and 1,52 ± 0,51 mm respectively.

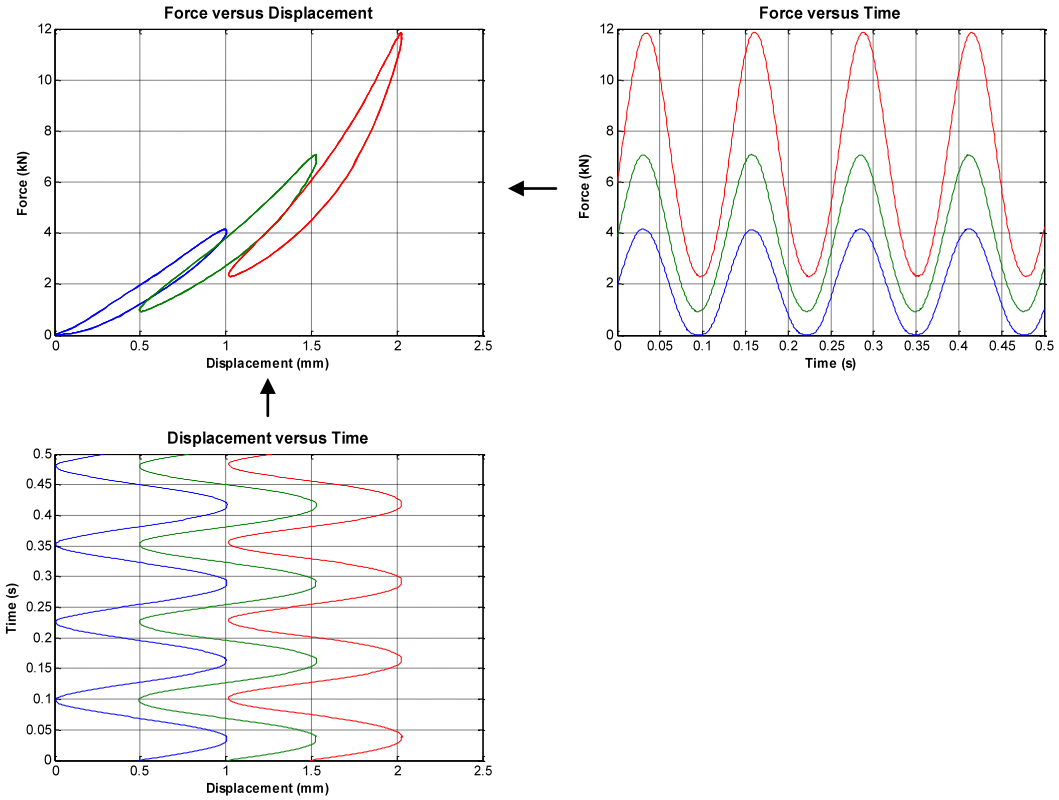

Figure 4-3: Measured data for CDM-46 at three preloads.

As can be seen from Figure 4-3, the excitation displacement is cyclic and the measured force has a similar profile. The figure shows the typical hysteresis loops that is generated as a viscoelastic material stores and releases energy. The transitional behaviour as the material goes from an unloaded to a loaded state is also slightly visible in the plots of the lowest force. This behaviour is particularly difficult to model and it can be attributed to the hydraulic cylinder losing contact with the material and/or force transducer.

4.6 Conclusion

This chapter gave an overview of the testing of viscoelastic materials. Three different materials were tested at three different preloads and excitation frequencies. The test setup, data acquisition system and data obtained were found to be useful and of good quality. For future work, it would be advisable to use a controller under force control with tests at higher frequencies and preloads as this is more comparable to the in situ conditions.

5 Optimisation

This chapter documents the processing of the experimental test data for the different materials. The main objective was to develop a simulation model and find the optimised parameters that predict the force a material generates as a function of the displacement and the velocity to which it is subjected.

5.1 Material models

Three material models were used and their parameters optimised using measured data as input. Special attention was paid to the material contact model and governing equations for a loss of contact were derived. The three models are based on the models found in Rivin (2003) and Maes et. al. (2006) with non-linearities added to account for the observed material behaviour. They are briefly discussed and presented in Figure 5-1 below:

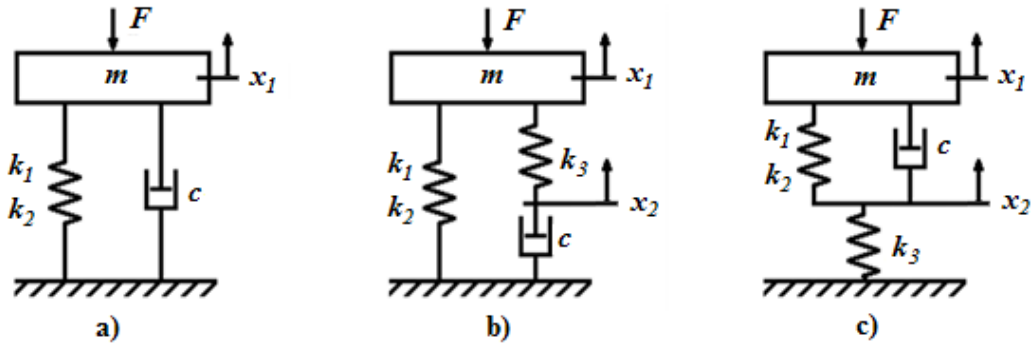

Figure 5-1: The final three different material models a) Non-linear, b) Relaxation and c) Creep.

5.1.1 General

All of the models feature at least three unknown material coefficients; these are stiffness coefficients (k_1, k_2, k_3) and a damping constant (c). The materials were subjected to a material displacement (x_1) and a relative displacement (x_2) which are dependent on the dynamics of the system. Under normal circumstances (typically high preloads), the material displacement is equal to the displacement of the hydraulic cylinder (d). Under certain circumstances, the material can lose contact with the cylinder and/or load cell and then the material displacement is calculated by using the dynamics of the system.

5.1.2 Cylinder-material contact criteria

The material displacement and velocity were constantly evaluated to confirm that the correct values were used. Under the following conditions, the material was in contact with the cylinder and/or load cell and would have the same displacement and velocity as the cylinder or load cell (i.e. $x_1 = d$, $\dot{x}_1 = v$):

- The cylinder is moving upward ($v > 0$) with a cylinder displacement greater than or equal to the material displacement ($d \geq x_1$).
- The cylinder displacement is greater than or equal to the material displacement ($d \geq x_1$) and the absolute cylinder velocity is less or equal to the absolute material velocity ($|v| \leq |\dot{x}_1|$).

If none of the above proved true, the material was found to have lost contact with the hydraulic cylinder and/or load cell. The velocity and displacement of the material was then calculated for each model as explained in the following sections. It should be kept in mind that this set of criteria is applicable for the layout of these specific material tests. When the material is used for rail pads, there are normally higher preloads present as the material is constrained by fasteners and the weight of the rail and/or train.

5.1.3 Non-linear model

This model is described as a simple spring-damper model with a non-linear, stiffening spring element. The equation for the transmitted force it generates is given below and it is presented in Figure 5-1a:

$$F_{trans} = k_1 x_1^3 + k_2 x_1 + c\dot{x}_1 \tag{5.1}$$

where k_1 and k_2 are the spring stiffness coefficient and c is a viscous damping constant.

As previously mentioned the fact that the cylinder and the material can lose contact had to be accounted for. In the event of this occurring, the material velocity and displacement are calculated as follows:

$$\dot{x}_1(t+\Delta t) = -\frac{1}{c}\left[k_1 x_1^3(t) + k_2 x_1(t)\right] \tag{5.2}$$

$$x_1(t+\Delta t) = x_1(t) + \Delta t \dot{x}_1(t+\Delta t) \tag{5.3}$$

5.1.4 Relaxation model

This model is described as a spring in parallel with a spring and damper. The equation for the transmitted force it generates is given below and it is presented in Figure 5-1b:

$$F_{trans} = k_1 x_1^3 + k_2 x_1 + k_3 (x_1 - x_2) \tag{5.4}$$

$$= k_1 x_1^3 + k_2 x_1 + c\dot{x}_2 \tag{5.5}$$

where k_1, k_2 and k_3 are spring stiffness coefficients and c is a viscous damping constant.

To determine x_2, the pseudo displacement, the following equation is solved:

$$\dot{x}_2 = \frac{k_3}{c}(x_1 - x_2) \tag{5.6}$$

As previously mentioned the fact that the cylinder and the material could lose contact had to be accounted for. In the event of this occurring, the material velocity and displacement are calculated as follows for this model:

$$x_1(t+\Delta t)=\frac{1}{k_2+k_3}\left[k_3x_2(t)-k_1x_1^3(t)\right] \tag{5.7}$$

$$\dot{x}_1(t+\Delta t)=\frac{x_1(t+\Delta t)-x_1(t)}{\Delta t} \tag{5.8}$$

$$\dot{x}_2(t+\Delta t)=-\frac{1}{c}\left[k_1x_1^3(t)+k_2x_1(t)\right] \tag{5.9}$$

$$x_2(t+\Delta t)=x_2(t)+\Delta t\dot{x}_2(t+\Delta t) \tag{5.10}$$

5.1.5 Creep model

This model is described as a spring and damper in series with a spring. The equation for the transmitted force it generates is given below and it is presented in Figure 5-1c:

$$F_{trans}=k_1\left(x_1^3-x_2^3\right)+k_2\left(x_1-x_2\right)x_1+c\left(\dot{x}_1-\dot{x}_2\right) \tag{5.11}$$

$$=k_3x_2 \tag{5.12}$$

where k_1, k_2 and k_3 are spring stiffness coefficients and c is a viscous damping constant.

To determine x_2, the pseudo displacement, the following equation has to be solved:

$$\dot{x}_2=\frac{1}{c}\left[k_1\left(x_1^3-x_2^3\right)+k_2\left(x_1-x_2\right)-k_3x_2+c\dot{x}_1\right] \tag{5.13}$$

As previously mentioned, the fact that the cylinder and the material could lose contact had to be accounted for. In the event of this occurring, the material velocity and displacement are calculated as follows:

$$x_2(t+\Delta t)=0 \tag{5.14}$$

$$\dot{x}_2(t+\Delta t)=\frac{-x_2(t)}{\Delta t} \tag{5.15}$$

$$\dot{x}_1(t+\Delta t)=\frac{1}{c}\left[-k_1x_1^3(t)-k_2x_1(t)+c\dot{x}_2(t)\right] \tag{5.16}$$

$$x_1(t+\Delta t)=x_1(t)+\Delta t\dot{x}_1(t+\Delta t) \tag{5.17}$$

5.2 Background to optimisation

Optimisation techniques are employed when a system has too many variables for the influence of each to be considered, and the system as a whole needs an optimal solution. In some cases, one can rely on experience and intuition to find this solution, but more complex problems needs structured and scientific approaches for problem solving. Various optimisation techniques are available and most techniques share the same basic terminology.

According to Vanderplaats (2005), numerical optimisation has the following advantages:

- Provides a faster design time.
- Provides a logical and systemised design procedure.
- Easily deals with an array of design variables and constraints.
- Yields an improved design.
- Requires minimal human-machine interaction.
- Removes bias as no intuition or previous experience is needed.

Keeping these factors in mind, it should be noted that numerical optimisation may not always provide an optimal solution and the results found may be misleading.

5.2.1 Objective function

The objective function is the function which is minimised and is dependent on the design variables of the problem or system. The objective function is usually denoted by $F(X)$ with X being the design variables, and it can be subject to certain constraints. When the objective function needs to be maximised, $-F(X)$ is minimised.

5.2.2 Constraints

The constraints on a system are the physical boundaries imposed on the system by design and are usually a function of the design variables. There are two types of

constraints: inequality constraints (denoted by *g(X)*) and equality constraints (denoted by *h(X)*). Additionally the design variables may be subject to constraints, referred to as side constraints. According to Vanderplaats (2005), these constraints can be symbolically described as follows:

$$g_j(X_i) \leq 0 \tag{5.18}$$

$$h_k(X_i) = 0 \tag{5.19}$$

$$X_i^l \leq X_i \leq X_i^u \tag{5.20}$$

5.2.3 Design variables

The design variables of a system are the variables which can be changed in the optimisation technique to change the objective function and constraints. The design variables can be subject to side constraints and are denoted by *X*.

5.2.4 Methodology

Most optimisation algorithms start off with an initial set of design variables (X^0) and the design variables are then updated iteratively. According to Vanderplaats (2005), this procedure can be described as follows:

$$X^q = X^{q-1} + \alpha * S^q \tag{5.21}$$

where q is the iteration number, α^* is the search distance and S is the search vector for a specific iteration.

S is chosen to reduce the objective function while maintaining the constraints and α^* is determined by numerical interpolation of a few chosen values for α^*. By following this procedure, a problem of n variables is reduced to a one-dimensional search problem. This is a general outline of the optimisation procedure and different algorithms utilise different methods of determining α^* and S.

The next problem encountered with an optimisation procedure is to determine whether the optimisation algorithm converges on an optimal solution. To determine whether these conditions are met, the search direction has to be both usable and feasible. Vanderplaats (2005) describes these requirements as follows:

$$\nabla F(X)^T S \leq 0 \tag{5.22}$$

$$\nabla g_j(X)^T S \leq 0 \tag{5.23}$$

5.3 Optimisation implementation

The objective function is seen as a constrained non-linear multivariable function. Optimisation of this function is achieved in Matlab R2008b by utilising the Optimization Toolbox™ V4.1 and using the `fmincon` function. `fmincon` is a sequential quadratic programming (SQP) method and updates an estimate of the Hessian matrix for each iteration by using the Broyden-Fletcher-Goldfarb-Shanno **(**BFGS) method.

As with all optimisation procedures, there is an objective function, equality constraints and inequality constraints. These inputs and outputs are discussed in more detail below:

5.3.1 Objective function

Since the calculated force (F_{calc}) or transmitted force have to be compared to the measured force (F_{meas}), the objective function takes the form of a quadratic error function. This function is then normalised by dividing it by the number of evaluated samples and peak/maximum force to make it comparable between the different material models and data record lengths. The error function has the following form:

$$E = \frac{1}{n}\sum_{i=1}^{n}\frac{\left(F_{i,calc} - F_{i,meas}\right)^2}{F_{max}} \tag{5.24}$$

where $F_{i,calc}$ is the force as calculated by the model, $F_{i,meas}$ is the measured force, F_{max} is the peak or maximum force and n is the total number of time steps evaluated.

In the case of the Relaxation and Creep models, there are two equations for the calculated force each containing different material constants. In order to contain

all the different material constants, the objective function was therefore calculated as the sum of the error functions of both calculated forces. As most of the models do not attain steady state operation from the start of their optimisation (due to numeric differentiation and integration), only the last 1,4 seconds (or 1920 samples) of the 4 seconds of data record was used to calculate the objective function (*n* was altered accordingly).

5.3.2 Constraints

The enforced constraints are quite simple: none of the material constants could be less than zero or greater than one thousand (for the stiffnesses) or one (for the damping). Material constants could not be negative as this would not be physically possible, and the upper limits were chosen respective to the existing material properties. Since the numerical integration uses division by the damping constant (*c*), this value could not be equal to zero as this would cause values approaching infinity. The constraints could be summarised as follows:

$$0 \le k_1 \le 10^{15} \tag{5.25}$$

$$0 \le k_2 \le 10^{9} \tag{5.26}$$

$$0 \le k_3 \le 10^{9} \tag{5.27}$$

$$10^{-3} \le c \le 10^{6} \tag{5.28}$$

5.3.3 Input data

The input data used for the optimisation procedure was the displacement of the hydraulic cylinder and corresponding generated force. The data was presented as a time series and the velocity of the cylinder was calculated as an additional input for the optimisation.

As previously mentioned, the cylinder-material contact conditions had to be checked as this would determine which displacement and velocity values were to be used.

5.3.4 Secondary calculations

During testing, the displacement and generated force exerted on the material was measured and recorded. Since some material properties such as damping are strain rate dependent, the velocity of the cylinder was required as well. The velocity is estimated numerically for the measured displacement by using the following formula:

$$v\left(t+\Delta t\right)=\frac{d\left(t+\Delta t\right)-d\left(t\right)}{\Delta t} \tag{5.29}$$

where d is the displacement of the cylinder and Δt is the time increment of data acquisition (0,833 milliseconds).

This numerical differentiation introduces some high frequency noise and discontinuities into the calculated velocity signal. A second order Low-pass Butterworth filter was used to remove most of these unwanted anomalies from the signal.

5.3.5 Optimisation procedure

The optimisation procedure consisted of two different step-wise processes. As can be seen in Figure 5-2 below, material displacements and velocities were calculated by using finite time steps and then recalculated for every change made to the design variables. The constraints placed on the design variables was enforced during the optimisation step.

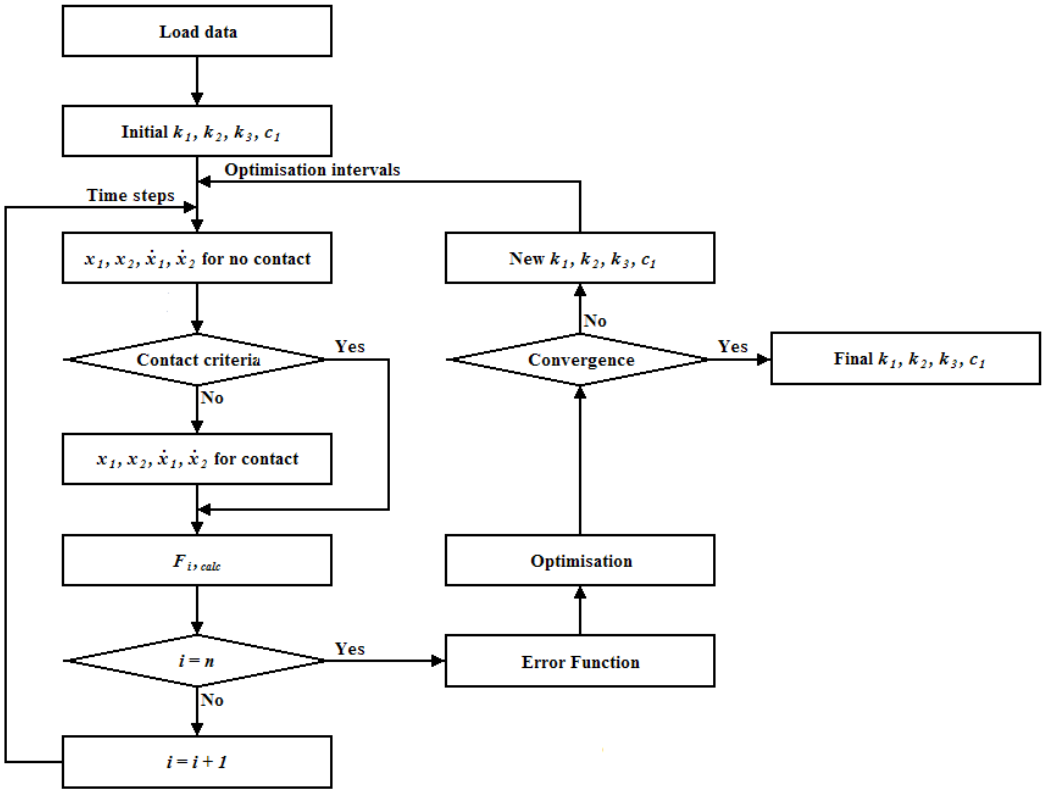

Figure 5-2: Optimisation procedure flow diagram.

5.4 Frequency and preload dependency

Since it proved difficult to obtain a single set of parameters to accurately describe the behaviour of a material under different preloads and excitation frequencies, the correlation between these parameters and conditions was investigated. Datasets were grouped according to preload or excitation frequency and a single objective function was calculated for the set as follows:

$$E_j = \sum_{i=1}^{N} E_i \qquad (5.30)$$

where E_j is the error function for a specific frequency or preload dataset, N is the number of datasets at a specific preload or frequency and E_i is the individual calculated error functions at the specific preload or frequency.

The values of the specific coefficients (k_1, k_2, k_3, c) were then normalised by dividing each coefficient by the maximum value of this coefficient obtained at the different preloads or frequencies. To gain an understanding of this process, refer to Table 5-1 below:

Table 5-1: Sample results for normalised coefficients for CDM-17.

Model	**Relaxation**			
Frequency (Hz)	**k_1**	**k_2**	**k_3**	**c**
4	1	0,69	0,81	1
8	0,93	0,72	0,89	0,54
16	0,62	1	1	0,30

When examining the coefficients in Table 5-1, it is obvious that k_1 and c had the biggest values at 4 Hz and the smallest values at 16 Hz. Therefore the coefficient for k_1 and c found at all frequencies was divided by these specific values. These normalised results were then plotted against the preload or frequency.

5.4.1 Frequency dependency

The Frequency dependency of the materials was examined and the results are presented in the tables and figures below:

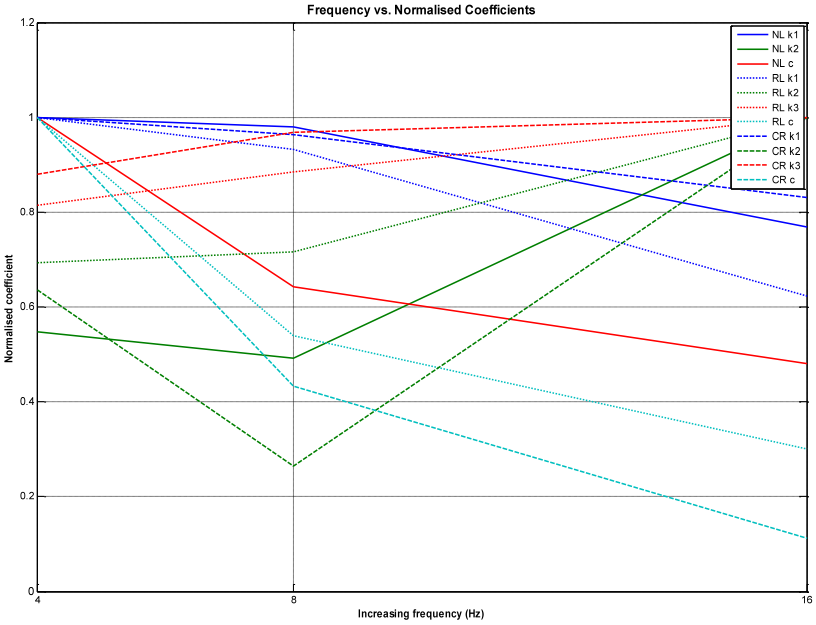

Figure 5-3: Normalised coefficients versus frequency for CDM-17.

Table 5-2: Normalised coefficients for CDM-17.

Model	**Non-linear**			**Relaxation**				**Creep**			
Frequency (Hz)	**k_1**	**k_2**	**c**	**k_1**	**k_2**	**k_3**	**c**	**k_1**	**k_2**	**k_3**	**c**
4	1	0,55	1	1	0,69	0,81	1	1	0,64	0,88	1
8	0,98	0,49	0,64	0,93	0,72	0,89	0,54	0,96	0,26	0,97	0,43
16	0,77	1	0,48	0,62	1	1	0,30	0,83	1	1	0,11

As can be seen from Figure 5-3 and Table 5-2 all of the coefficients except the Non-linear k_2 and Creep k_2 shows some form of frequency dependency. In general k_1 and c decrease with frequency while k_2 and k_3 increase as higher excitation frequencies are applied.

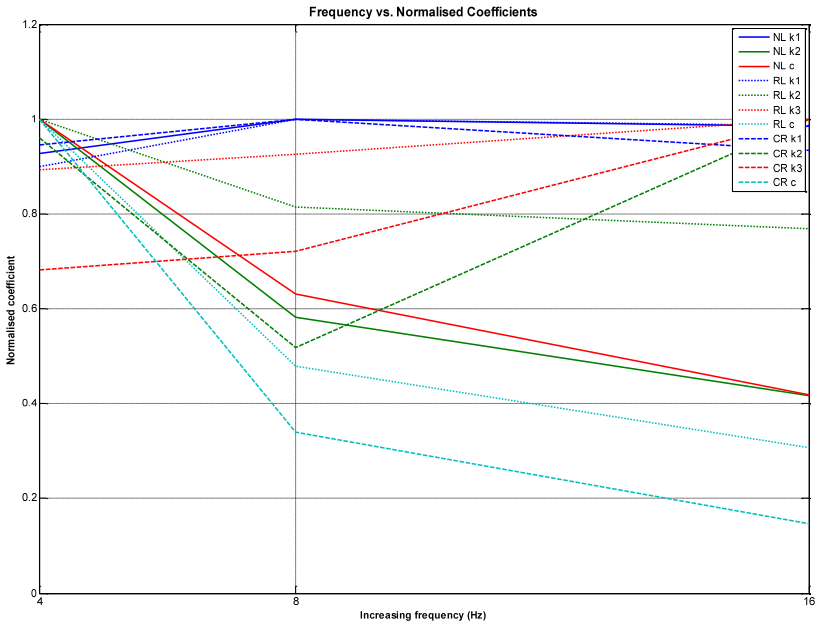

Figure 5-4: Normalised coefficients versus frequency for CDM-45.

Table 5-3: Normalised coefficients for CDM-45.

Model	**Non-linear**			**Relaxation**				**Creep**			
Frequency (Hz)	**k_1**	**k_2**	**c**	**k_1**	**k_2**	**k_3**	**c**	**k_1**	**k_2**	**k_3**	**c**
4	0,93	1	1	0,90	1	0,89	1	0,94	0,96	0,68	1
8	1	0,58	0,63	1	0,82	0,93	0,48	1	0,52	0,72	0,34
16	0,99	0,42	0,42	0,99	0,77	1	0,31	0,93	1	1	0,15

As can be seen from Figure 5-4 and Table 5-3 all of the coefficients except all the k_1's and Creep k_2 show some form of frequency dependency. In general, c decreases with frequency.

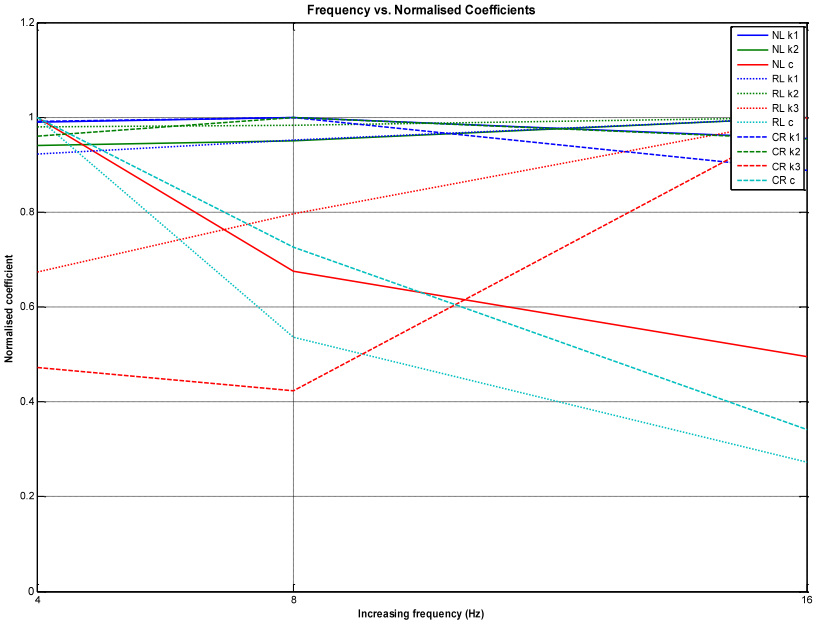

Figure 5-5: Normalised coefficients versus frequency for CDM-46.

Table 5-4: Normalised coefficients results for CDM-46.

Model	Non-linear			Relaxation				Creep			
Frequency (Hz)	**k_1**	**k_2**	**c**	**k_1**	**k_2**	**k_3**	**c**	**k_1**	**k_2**	**k_3**	**c**
4	0,99	0,94	1	0,92	0,98	0,67	1	0,99	0,96	0,47	1
8	1	0,95	0,68	0,95	0,98	0,80	0,54	1	1	0,42	0,73
16	0,96	1	0,50	1	1	1	0,27	0,89	0,95	1	0,34

As can be seen from Figure 5-5 and Table 5-4 most of the coefficients show some form of frequency dependency or stay fairly constant as the excitation frequency increases. In general, k_1 and k_2 show no change and c decreases with frequency.

5.4.2 Preload dependency

The preload dependency of the materials is examined and the results are presented in the tables and figures below:

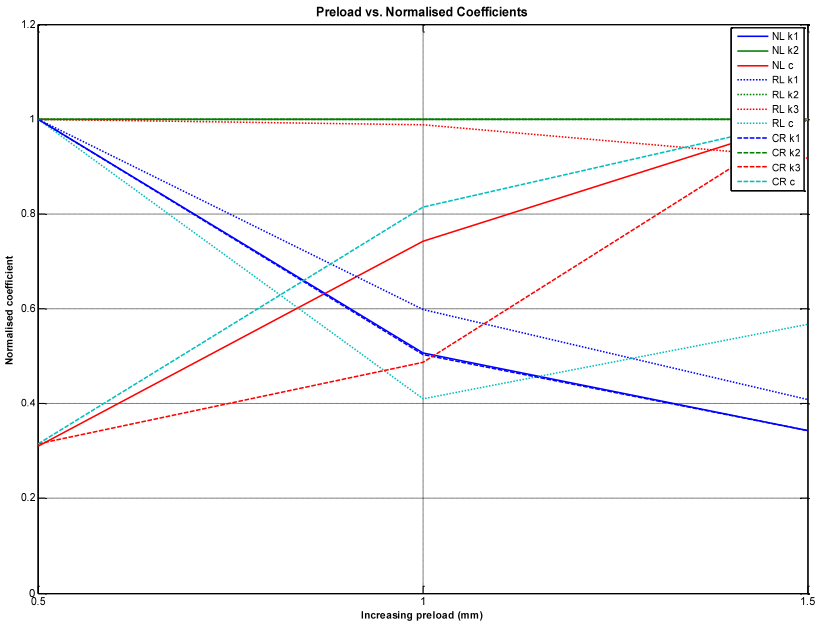

Figure 5-6: Normalised coefficients versus preload for CDM-17.

Table 5-5: Normalised coefficients for CDM-17.

Model	**Non-linear**			**Relaxation**				**Creep**			
Preload (mm)	**k_1**	**k_2**	**c**	**k_1**	**k_2**	**k_3**	**c**	**k_1**	**k_2**	**k_3**	**c**
0,5	1	1	0,31	1	1	1	1	1	1	0,31	0,31
1	0,51	1	0,74	0,60	1	0,99	0,41	0,50	1	0,49	0,81
1,5	0,34	1	1	0,41	1	0,92	0,57	0,34	1	1	1

As can be seen from Figure 5-6 and Table 5-5 most of the coefficients show some form of preload dependency or stay fairly constant as the preload increases. In general, k_1 decreases with preload, k_2 shows no change (in reality it could be zero) and c, as well as k_3, increases as the preload rises.

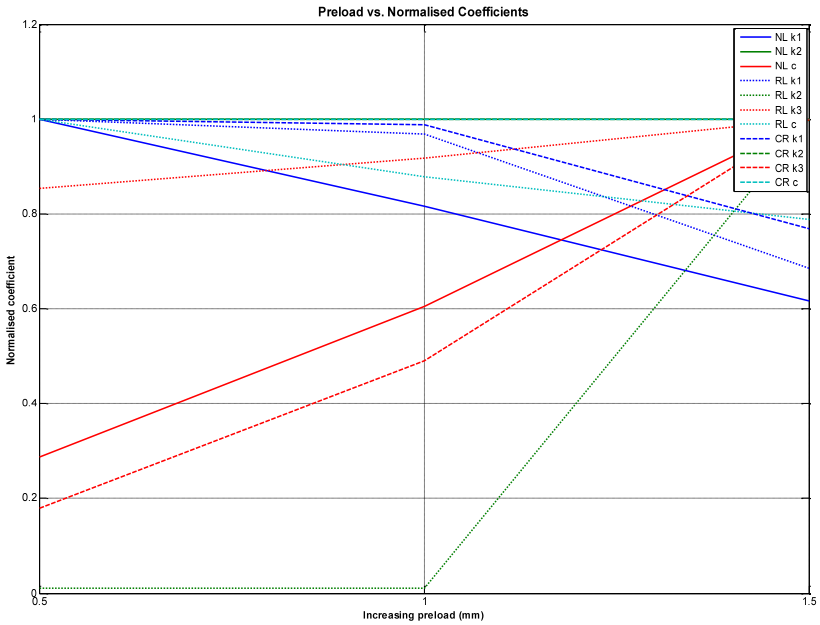

Figure 5-7: Normalised coefficients versus preload for CDM-45.

Table 5-6: Normalised coefficients results for CDM-45.

Model	**Non-linear**			**Relaxation**				**Creep**			
Preload (mm)	**k_1**	**k_2**	**c**	**k_1**	**k_2**	**k_3**	**c**	**k_1**	**k_2**	**k_3**	**c**
0,5	1	1	0,29	1	0,01	0,85	1	1	1	0,18	1
1	0,82	1	0,61	0,97	0,01	0,92	0,88	0,99	1	0,49	1
1,5	0,62	1	1	0,68	1	1	0,79	0,77	1	1	1

As can be seen from Figure 5-7 and Table 5-6 most of the coefficients show some form of preload dependency or stay fairly constant as the preload increases. In general, k_1 decreases with preload, k_2 exhibits no change (in reality it could be zero), k_3 increases and c has no real general trend.

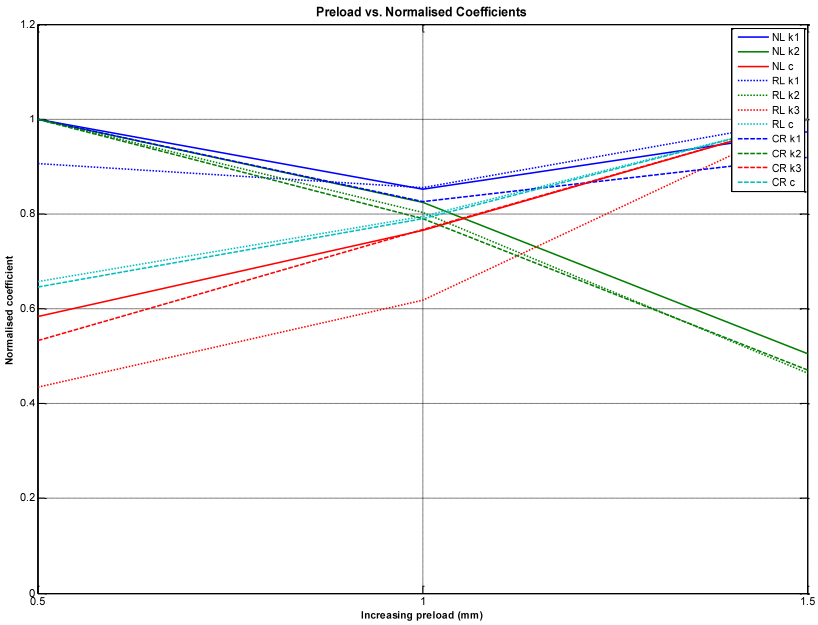

Figure 5-8: Normalised coefficients versus preload for CDM-46.

Table 5-7: Normalised coefficients results for CDM-46.

Model	**Non-linear**			**Relaxation**				**Creep**			
Preload (mm)	**k_1**	**k_2**	**c**	**k_1**	**k_2**	**k_3**	**c**	**k_1**	**k_2**	**k_3**	**c**
0,5	1	1	0,58	0,91	1	0,43	0,66	1	1	0,53	0,65
1	0,85	0,82	0,76	0,86	0,80	0,62	0,79	0,83	0,79	0,77	0,79
1,5	0,97	0,51	1	1	0,46	1	1	0,92	0,47	1	1

As can be seen from Figure 5-8 and Table 5-7 most of the coefficients show some form of preload dependency. In general, k_1 and k_2 decrease with preload while k_3 and c increase as higher preloads are applied.

5.5 Sample results

5.5.1 Case 1: CDM-17 at low preload and 8 Hz excitation

Case 1 is a 10 mm sample of CDM-17 tested at 8 Hz with a 0,5 mm preload applied to the material, and the optimisation applied to this dataset alone. The results of this optimisation are shown in Figure 5-9 and Table 5-8 below:

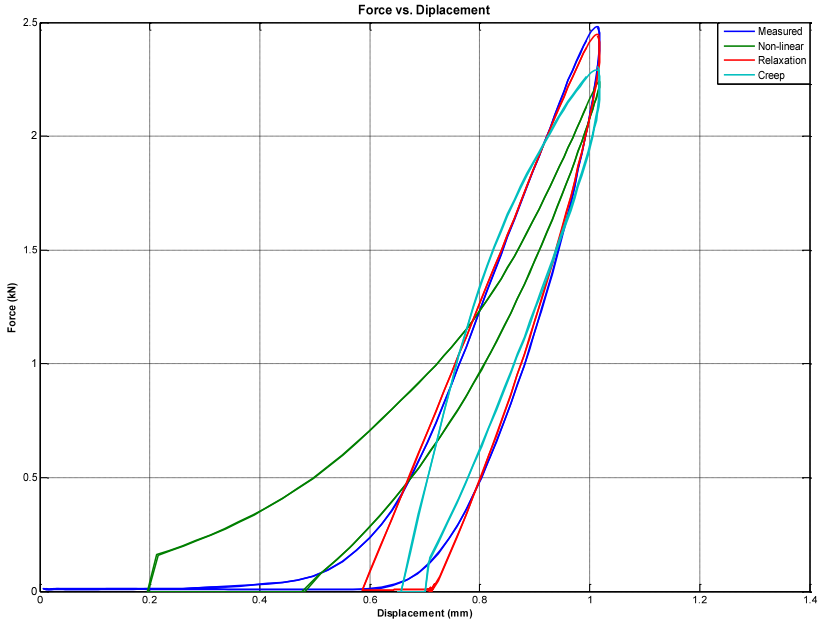

Figure 5-9: Force versus displacement for CDM-17.

Table 5-8: Optimisation results for CDM-17.

Model	k_1 **[10^{12} N/m^3]**	k_2 **[10^6 N/m]**	k_3 **[10^6 N/m]**	c **[10^6 Ns/m]**	**Error [10^3]**
Non-linear	2,087	0	n.a.	0,008	9,15
Relaxation	1,578	0	3,85	0,131	0,23
Creep	0,242	0,18	6,64	0,248	2,09

As can be seen in Figure 5-9 and Table 5-8, only the Non-linear model comes close to describing the transitional behaviour at low preload conditions. The Relaxation and Creep models give quite accurate representations of the material

when the forces are not in the transition from load to no-load. When considering the size of the errors, the Relaxation model is by far the most accurate model with the data suggesting it is nine times more accurate than the Creep model and almost forty times more accurate than the Non-linear model. It would appear that k_2 has little effect on the model as the values are small compared with the other stiffnesses.

To better interpret the force versus displacement plot, we need to examine the force and displacement separately as a function of time.

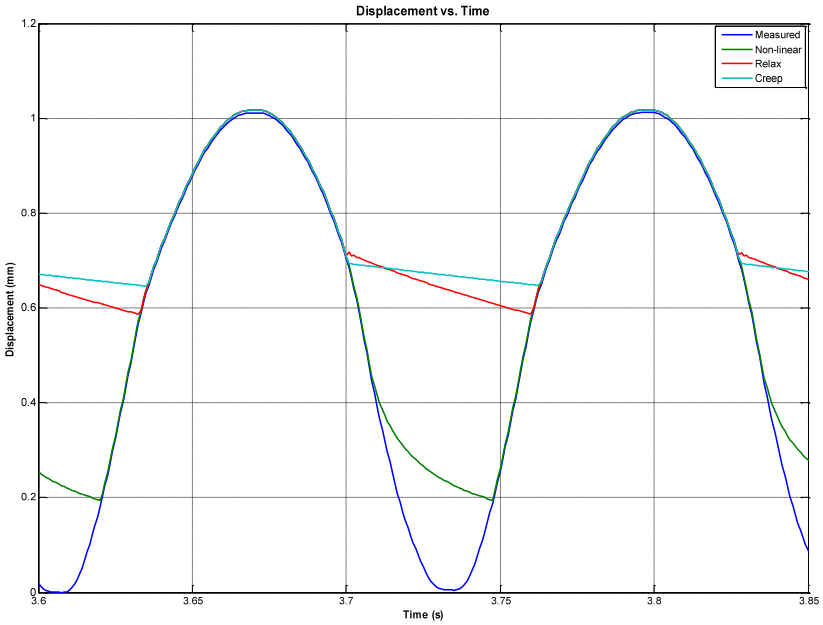

Figure 5-10: Displacement versus time for CDM-17.

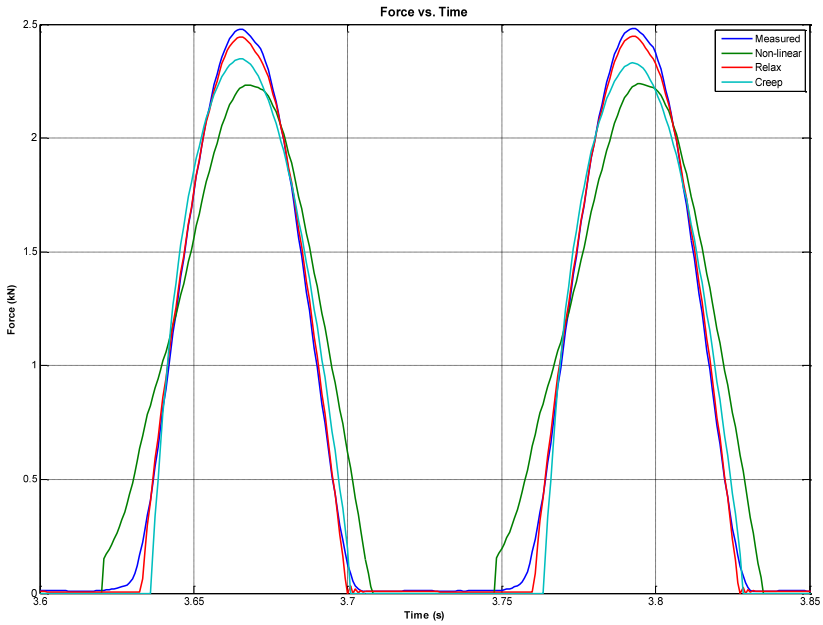

Figure 5-11: Force versus time for CDM-17.

As can be seen from Figure 5-10 and Figure 5-11 all the different models experience conditions in which the cylinder and materials lose contact. The Non-linear model enables the material to keep contact with the cylinder longer than the Relaxation and Creep models, but the transmitted forces of these two models are more representative of the measured forces. The Relaxation model seems to best model the measured force even though Figure 5-9 might suggest otherwise.

5.5.2 Case 2: CDM-17 at low preload and 8 Hz excitation

Case 2 is a 10 mm sample of CDM-17 tested at 8 Hz with a 0,5 mm preload applied to the material and the optimisation applied to all the datasets (i.e. one set of parameters was sought for all the tests). The result of this optimisation is shown in Figure 5-12 and Table 5-9 below:

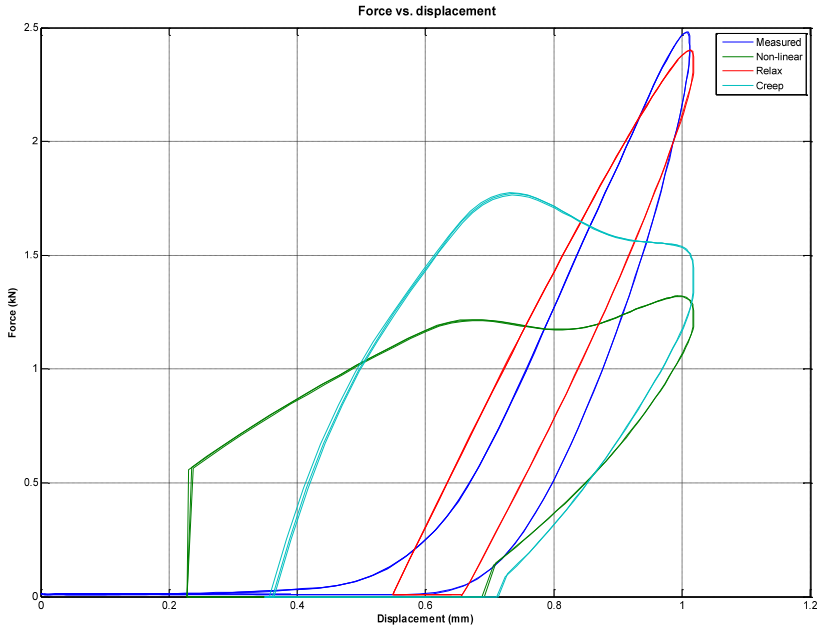

Figure 5-12: Force versus displacement for CDM-17.

Table 5-9: Optimisation results for CDM-17.

Model	k_1 **[10^{12} N/m^3]**	k_2 **[10^6 N/m]**	k_3 **[10^6 N/m]**	c **[10^6 Ns/m]**	**Error [10^3]**
Non-linear	0,661	0,434	n.a.	0,024	62,42
Relaxation	0,380	0,917	4,276	0,253	2,37
Creep	0,650	0,473	10,536	0,048	56,28

As can be seen in Figure 5-12 and Table 5-9 only the Relaxation model provides decent representation the tested data. The values of k_1, k_2, k_3 and c are vastly different to those found in Case 1 which used the same measured data for the optimisation procedure. When considering the errors, the Relaxation model is by far the most accurate model with the data suggesting it is up to twenty-three times more accurate than the Creep model and Non-linear model.

To better interpret the Force versus displacement plot, we need to examine the force and displacement separately as a function of time.

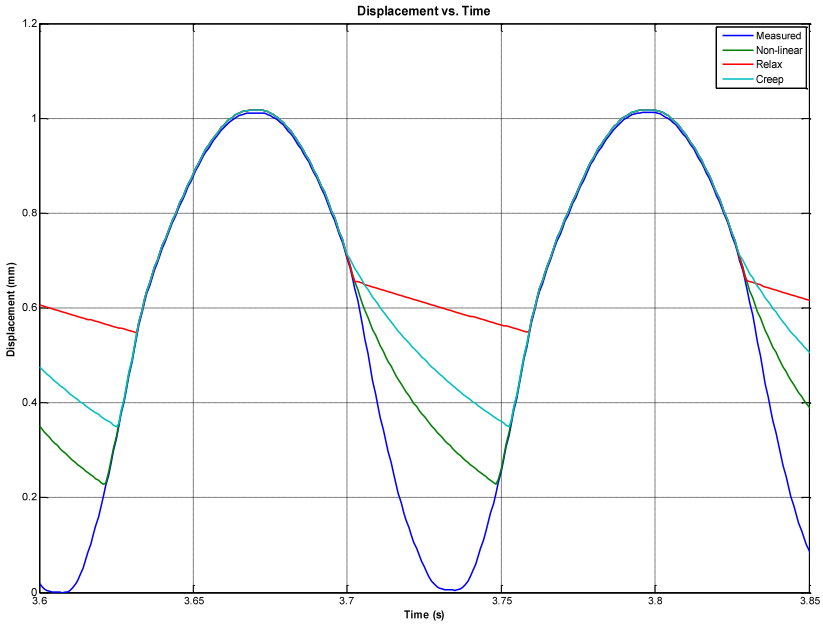

Figure 5-13: Displacement versus time for CDM-17.

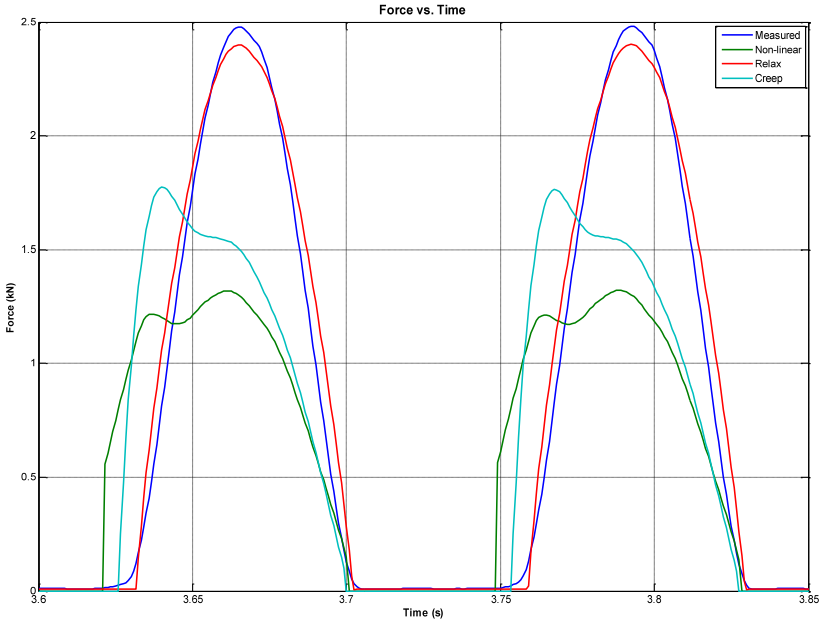

Figure 5-14: Force versus time for CDM-17.

As can be seen from Figure 5-13 and Figure 5-14 all the different models experience conditions in which the cylinder and materials lose contact. These

conditions all appear at the same time. The Relaxation model is the only model to accurately model the measured force with the Non-linear and Creep models being completely unsuitable. As can be seen from Figure 5-14, the transition from no-load to load conditions are difficult to capture and represent with any of the models.

Since this optimisation was carried out on all datasets, we need to examine the results obtained at other load cases. This data is presented as the errors at the different load cases in Table 5-10 below:

Table 5-10: Optimisation results for CDM-17 at all load cases.

Preload (mm)	Frequency (Hz)	Error [103]		
		Non-linear	Relaxation	Creep
0,5	4	76,55	7,01	77,33
0,5	8	62,42	2,37	56,28
0,5	16	54,97	5,36	23,06
1	4	20,11	2,43	21,55
1	8	21,07	1,12	19,02
1	16	14,32	7,18	3,33
1,5	4	11,33	2,40	11,24
1,5	8	8,92	2,20	7,55
1,5	16	8,51	7,44	12,78

When analysing the data in Table 5-10, it is clear that a single set of coefficients is not adequate to describe the material characteristics at different preloads and excitation frequencies. It can also be observed that the model struggles with the prediction of forces at low preloads as these errors are up to twenty-three times higher than the errors at higher preloads.

5.5.3 Case 3: CDM-45 at high preload and 16 Hz excitation

Case 3 is a 10 mm sample of CDM-45 tested at 16 Hz with a 1,5 mm preload applied to the material and the optimisation applied to this dataset alone. The result of this optimisation is shown in Figure 5-15 and Table 5-11 below:

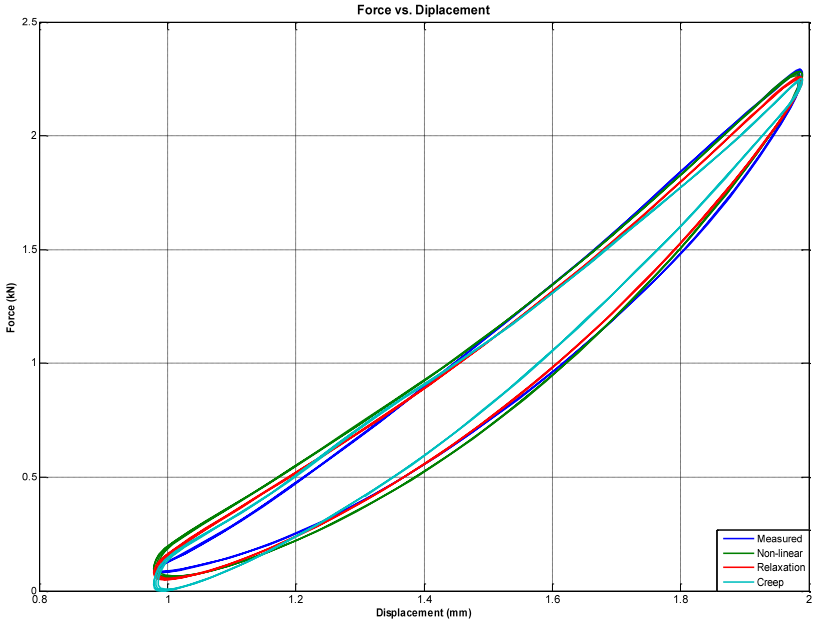

Figure 5-15: Force versus displacement for CDM-45.

Table 5-11: Optimisation results for CDM-45.

Model	k_1 **[10^{12} N/m^3]**	k_2 **[10^6 N/m]**	k_3 **[10^6 N/m]**	c **[10^6 Ns/m]**	**Error [10^3]**
Non-linear	0,271	0	n.a.	0,005	0,23
Relaxation	0,243	0,069	0,708	0,009	0,18
Creep	0,238	0,103	4,968	0,008	0,67

As can be seen in Figure 5-15 and Table 5-11, all the models provide a good representation of the tested data. When considering the errors, the Relaxation model is by far the most accurate model with the data suggesting it is almost four times more accurate than the Non-linear model. It is interesting to note that the values for k_1 and c are of the same order for all the models and the models seem more suited for implementation at higher preloads.

5.5.4 Case 4: CDM-46 at high preload and 4 Hz excitation

Case 4 is a 10 mm sample of CDM-46 tested at 4 Hz with a 1,5 mm preload applied to the material and the optimisation applied to all the datasets (i.e. one set of parameters was sought for all preloads and excitation frequencies). The result of this optimisation is shown in Figure 5-16 and Table 5-12 below:

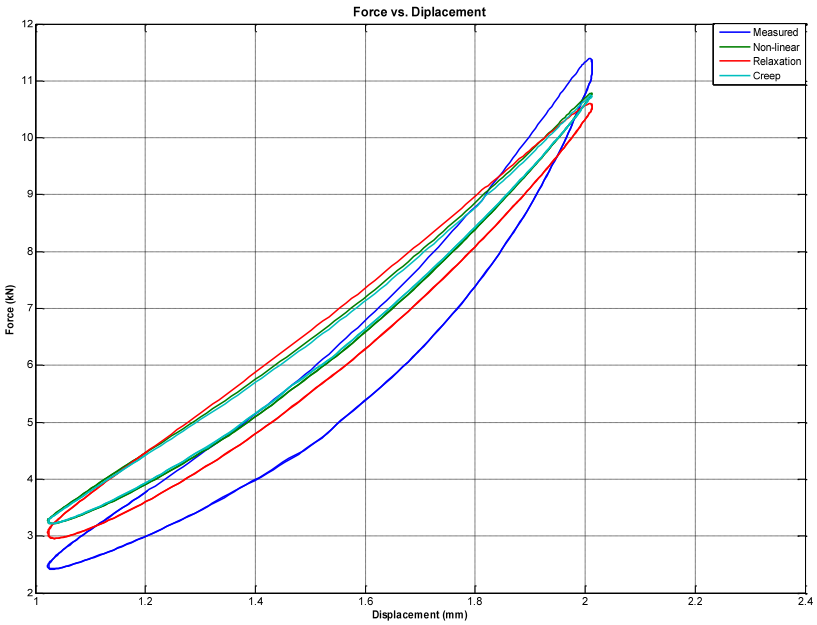

Figure 5-16: Force versus displacement for CDM-46.

Table 5-12: Optimisation results for CDM-46.

Model	k_1 **[10^{12} N/m^3]**	k_2 **[10^6 N/m]**	k_3 **[10^6 N/m]**	c **[10^6 Ns/m]**	**Error [10^3]**
Non-linear	0,705	2,491	n.a.	0,025	3,95
Relaxation	0,623	2,631	2,664	0,057	2,84
Creep	0,749	2,675	38,267	0,028	3,99

As can be seen in Figure 5-16 and Table 5-12, all the models provide decent representations of the tested data. When considering the errors, the models seem to fare equally well at predicting the response. A cause for concern is the fact that k_3 for the Creep model is significantly higher than the values obtained for the Non-linear and Relaxation models.

Since this optimisation was carried out on all datasets, we need to examine the results obtained at other load cases. This data is presented as the errors at the different load cases in Table 5-13 below:

Table 5-13: Optimisation results for CDM-46 at all load cases.

Preload (mm)	Frequency (Hz)	Error [10^3]		
		Non-linear	Relaxation	Creep
0,5	4	12,17	7,07	11,91
0,5	8	11,18	4,26	10,75
0,5	16	6,24	4,71	5,62
1	4	1,65	0,55	1,69
1	8	1,29	1,14	1,29
1	16	2,59	4,01	2,81
1,5	4	3,95	2,84	3,99
1,5	8	3,40	1,77	3,47
1,5	16	1,60	1,91	1,77

When observing the data in Table 5-13, it is clear that a single set of coefficients is not adequate to describe the material characteristics at different preloads and excitation frequencies. It can also be observed that the model struggles with the prediction of forces at low preloads as these errors are up to fourteen times higher than the errors at higher preloads.

5.5.5 Case 5: CDM-17 at high preload and 4 Hz excitation

Case 5 is a 10 mm sample of CDM-17 tested at 4 Hz with a 1,5 mm preload applied to the material and the optimisation applied to all the datasets with the same excitation frequencies (i.e. one set of parameters was sought for a set excitation frequency). The result of this optimisation is shown in Figure 5-17 and Table 5-14 below:

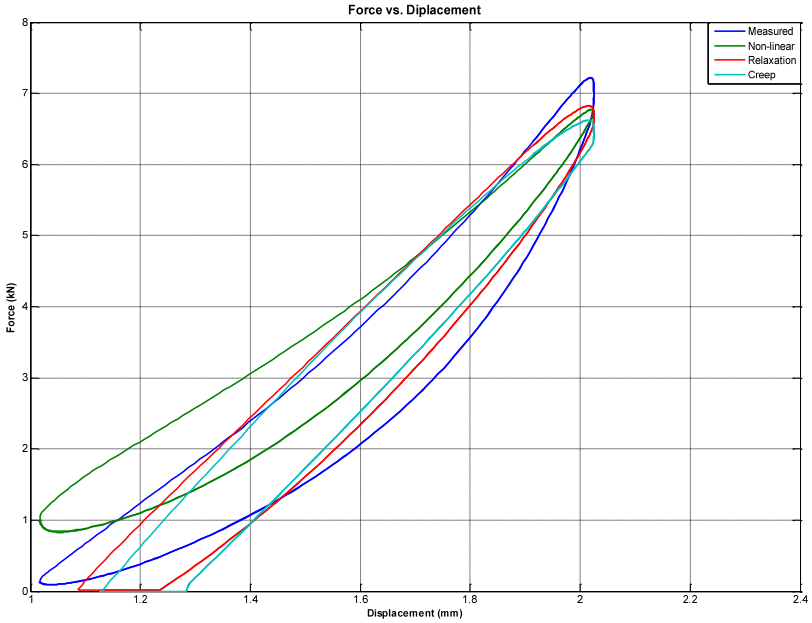

Figure 5-17: Force versus displacement for CDM-17.

Table 5-14: Optimisation results for CDM-17.

Model	k_1 [10^{12} N/m^3]	k_2 [10^6 N/m]	k_3 [10^6 N/m]	c [10^6 Ns/m]	**Error** [10^3]
Non-linear	0,724	0,34	n.a.	0,046	8,91
Relaxation	0,444	0,789	4,162	0,342	1,43
Creep	0,562	0,363	8,926	0,545	2,75

As can be seen in Figure 5-17 and Table 5-14, none of the models provides a decent representation of the experimental data. The Relaxation model provides the best estimation of the physical force. Since this optimisation was carried out on all datasets at the same excitation frequency, we need to examine the results obtained at other the other preloads. This data is presented as the errors at the different preloads in Table 5-15 below:

Table 5-15: Optimisation results for CDM-17 at same frequency.

Preload (mm)	Error [10^3]		
	Non-linear	Relaxation	Creep
0,5	82,86	2,95	3,04
1	16,77	0,80	2,89
1,5	8,91	1,43	2,75

When observing the data in Table 5-15, it is clear that a single set of coefficients is not adequate to describe the material characteristics at a specific excitation frequency.

5.5.6 Case 6: CDM-45 at low preload and 8 Hz excitation

Case 5 is a 10 mm sample of CDM-45 tested at 8 Hz with a 0,5 mm preload applied to the material and the optimisation applied to all the datasets with the same preload (i.e. one set of parameters was sought for a set preload). The result of this optimisation is shown in Figure 5-18 and Table 5-16 below:

Table 5-16: Optimisation results for CDM-45.

Model	k_1 [10^{12} N/m^3]	k_2 [10^6 N/m]	k_3 [10^6 N/m]	c [10^6 Ns/m]	Error [10^3]
Non-linear	0,436	0,001	n.a.	0,002	6,55
Relaxation	0,334	0,001	0,61	0,024	2,30
Creep	0,347	0,001	1,221	0,008	11,82

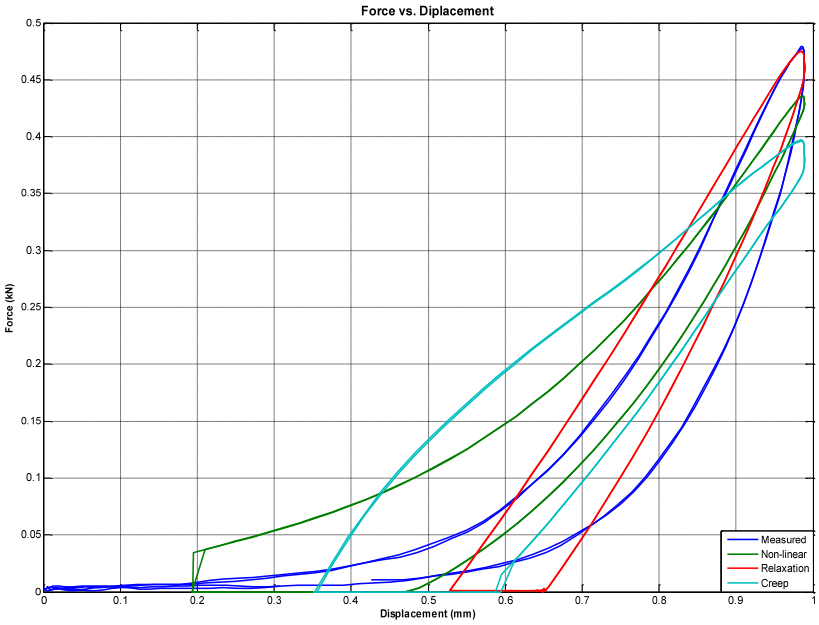

Figure 5-18: Force versus displacement for CDM-45.

As can be seen in Figure 5-18 and Table 5-16, only the Non-linear model comes close to describing the transitional behaviour at low preload conditions. The Relaxation and Creep models give quite accurate representations of the material when the forces are not in the transition from load to no-load. When considering the errors, the Relaxation model is by far the most accurate model with the data suggesting it is five times more accurate than the Creep model and almost three times more accurate than the Non-linear model. It would appear that k_2 has little effect on the model as the values are small compared with the other stiffnesses.

To better interpret the force versus displacement plot, we need to examine the force and displacement separately as a function of time.

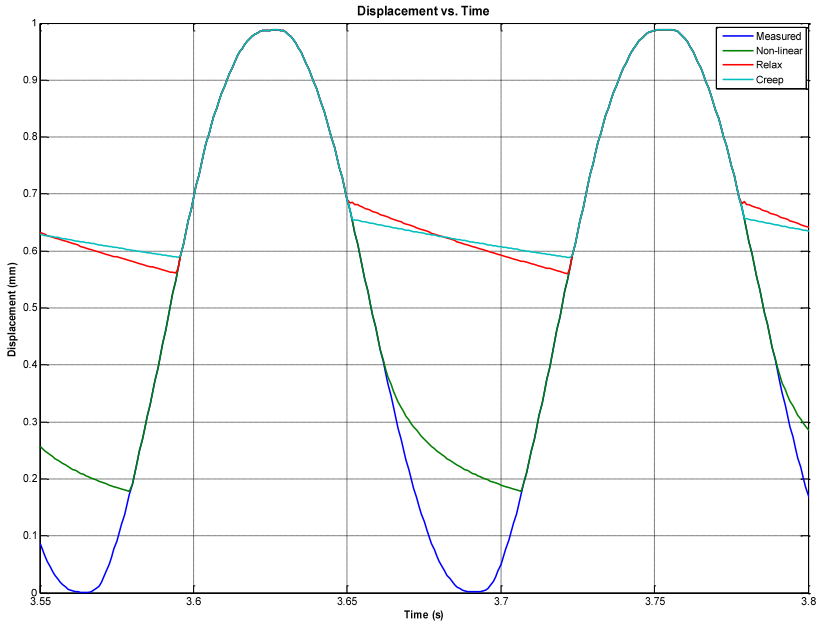

Figure 5-19: Displacement versus time for CDM-45.

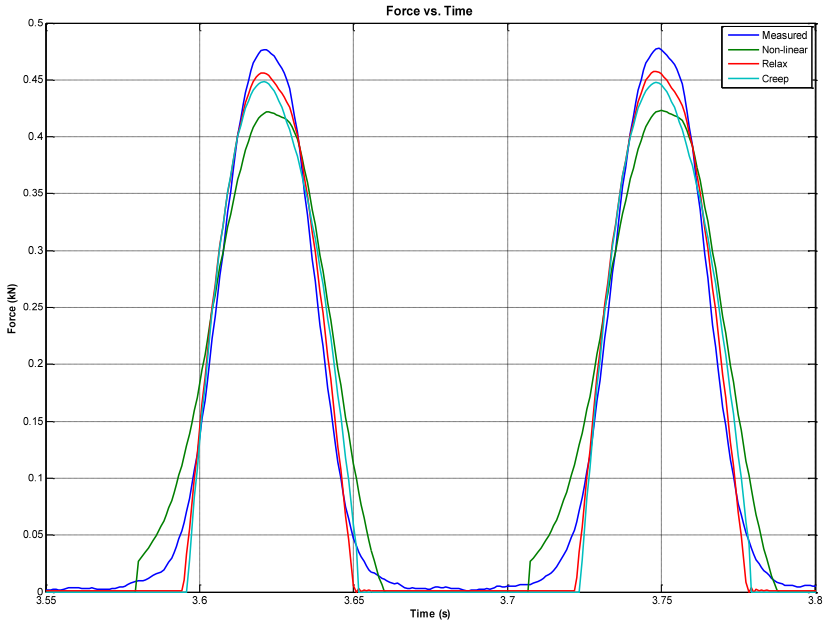

Figure 5-20: Force versus time for CDM-45.

As can be seen in Figure 5-19 and Figure 5-20 all the different models experience conditions in which the cylinder and materials lose contact. The Non-linear model enables the material to keep contact with the cylinder longer than the Relaxation and Creep models, but the transmitted forces of these two models are more

representative of the measured forces. The Relaxation and Creep model would seem to model the measured force the best even though the Figure 5-18 might suggest otherwise. As can be seen from Figure 5-20, the transition from no-load to load conditions is difficult to capture and represent with any of the models.

Since this optimisation was carried out on all datasets at the same preload, we need to examine the results obtained at other the other excitation frequencies. This data is presented as the errors at the different frequencies in Table 5-17 below:

Table 5-17: Optimisation results for CDM-45 at same preload.

Frequency (Hz)	Error [10^3]		
	Non-linear	Relaxation	Creep
4	4,73	3,08	10,89
8	6,55	2,30	11,82
16	5,72	4,74	14,50

When observing the data in Table 5-17, it is clear that a single set of coefficients is not adequate to describe the material characteristics at a specific preload.

5.6 Conclusion

This chapter is an overview of the development of material models and the subsequent optimisation of these models. The models are presented in detail and some typical optimisation results are shown. It can be concluded that it would be impossible to find a single set of material parameters for all excitation frequencies and preloads. The relationship between material parameters and frequency as well as preload was investigated to determine if this could be a viable solution to the problem.

The Relaxation model is consistently the best model when comparing the errors and this model should be used in future work.

6 Conclusions and recommendations

The following conclusions can be drawn from the work done in this study. Some recommendations are also supplied for future work and similar projects. The main conclusions to be drawn are:

- **A Relaxation model with a non-linear spring element provides the best prediction of transmitted forces in a viscoelastic material.**
- **A single set of coefficients is not adequate to describe the material characteristics for various excitations and preloads.**
- **The models generated are ideally suited for use when conditions are similar to those experienced physically by rail pads (high preloads and frequencies).**

Literature study

Some of the following conclusions can be drawn with regard to the literature study conducted:

- A wide variety of systems is available to reduce the vibration and noise generated by rail transport with most of these systems utilising resilient elements.
- Rail pads are one of easiest and most common solutions to implement to reduce rail vibrations.
- Many authors have generated and implemented track models with various different methods used to solve them and to represent the loads and components presented in the models.
- Most authors concluded that there is a major difficulty in obtaining material parameters and properties that are applicable to a wide range of conditions.

Material testing

The following conclusions are drawn with regards to the material testing conducted:

- The test procedure implemented to determine the physical characteristics of a resilient material is appropriate.
- It was found that displacement control is not an ideal method to control this type of testing and that force control would have been a more suitable method to guarantee better repeatability.
- Since the different materials were not tested at high excitation frequencies and preloads, no real conclusion can be drawn about the material behaviour at these conditions.

Material models

From the material models generated, the following conclusions can be drawn:

- Three different material models were generated, each incorporating spring (linear and non-linear) and damper elements as well as compensation for when the material loses surface contact.
- The Relaxation model proved to be the most reliable and accurate model to predict the transmitted forces and the Creep model was found to be the least accurate model.
- The cylinder-material contact criteria might not be applicable to real installations of the materials since higher preloads are present and the models fare better at predicting forces under these conditions than are found in reality.

Optimisation

The optimisation implemented leads to the following conclusions:

- The optimisation procedure used to determine the coefficients of the material model is satisfactory.

- It was found that Matlab and the Optimization Toolbox™ V4.1 provided a stable and easy to implement platform for running basic optimisation problems.
- The cylinder-material contact criteria added unwanted complexity to the system at higher preloads when it is not really applicable.
- It was found that the material coefficients have some form of preload dependency, but more data and optimisation is needed to prove this.
- The optimisation procedure is very successful at higher preloads, but the non-linearity introduced by the contact criteria cause difficulty at lower preloads with transitional behaviour.

Recommendations

A few recommendations can be made for future work with similar scopes.

- More testing can be done at higher preloads and frequencies as these conditions are more applicable to the real use of the materials.
- A more statistical approach to the testing of the material could be implemented.
- Force control for the material testing could provide better repeatability and control.
- Different optimisation algorithms and programs can be explored to determine if better results can be achieved.

7 References

Adhikari, S. 1998. Damping Models for Structural Vibration. *Journal of Sound and Vibration.* Vol. 215, 547 – 569.

Adhikari, S. and Woodhouse, J. 2000. Towards Identification of a General Model of Damping. *Proceedings of the 18th International Modal Analysis Conference*. 377 - 383.

Adhikari, S. and Woodhouse, J. 2001. Identification of Damping: Part I & II, *Journal of Sound and Vibration.* Vol. 243(1), 43 - 61 & 63 - 88.

Alvelid, M. and Enelund, M. 2007. Modelling of constrained thin rubber layer with emphasis on damping. *Journal of Sound and Vibration*. Vol. 300, 662 - 675.

Bandstra, J.P. 1983. Comparison of Equivalent Viscous Damping and Non-linear Damping in Discrete and Continuous Vibrating Systems. *Journal of Vibration, Acoustics, Stress, Reliability in Design*. Vol. 105, 382 - 392.

British Standards Institution. Evaluation and measurement for vibration in buildings – Part 1: Guide for measurement of vibrations and evaluation of their effects on buildings. BS 7385-1:1990.

Carrascal, I.A., Casado, J.A., Polanco, J.A. and Gutiérrez-Solana, F. 2007. Dynamic behaviour of railway fastening setting pads. *Engineering Failure Analysis.* Vol. 14, 364 - 373.

Cartmell, M. 1990. Introduction to Linear, Parametric and Non-linear Vibrations. London: Chapman and Hall.

Castellani, A. 2000. Vibrations Generated by Rail Vehicles: A Mathematical Model in the Frequency Domain. *Vehicle System Dynamics.* Vol. 34, 153 - 173.
CDM-Solids Catalogue. 2006. Overijse: CDM

Cox, S.J., Wang, A., Morison, C., Carels, P., Kelly, R. and Bewes, O.G. 2006. A test rig to investigate slab track structures for controlling ground vibration, *Journal of Sound and Vibration.* Vol. 293, 901 - 909.

Dall'Asta, A. and Ragni, L. 2006. Experimental tests and analytical model of high damping rubber dissipating devices. *Engineering Structures.* Vol. 28, 1874 - 1884.

Elastic solutions for track superstructure. 2002. Getzner Werkstoffe GmbH, Bürs.

Fiala, P., Degrande, G. and Augusztinovicz, F. Numerical modelling of ground-borne noise and vibration in buildings due to surface rail traffic. *Journal of Sound and Vibration.* Vol. 301 (2007), 718 - 738.

Guigou-Carter, C., Villot, M., Guillerme, B. and Petit, C. 2006. Analytical and experimental study of sleeper SAT S 312 in slab track Sateba system. *Journal of Sound and Vibration.* Vol. 293, 878 - 887.

Heckl, M., Hauck, G. and Wettsschureck, R. 1996. Structure-borne Sound and Vibration from rail traffic. *Journal of Sound and Vibration.* Vol. 193(1), 175 -184.

Kaewunruen, S. and Remennikov, A.M. 2006. Sensitivity analysis of free vibration characteristics of an in situ railway concrete sleeper to variations of rail pad parameters. *Journal of Sound and Vibration.* Vol. 298, 453 - 461.

Karlström, A. and Boström, A. 2006. An analytical model for train-induced ground vibrations from railways. *Journal of Sound and Vibration.* Vol. 292, 221 - 241.

Krüger, F. and Girnau, G. 2007. *Local and regional railway tracks in Germany.* Dusseldorf: Alba Fachverlag.

Inman, D.J. 2001. *Engineering Vibration.* Upper Saddle River: Prentice Hall International.

International Organisation for Standardisation. Acoustics and vibration – Laboratory measurement of vibro-acoustic transfer properties of resilient elements. ISO 10846-1 to 3:1997.

International Organisation for Standardisation. Mechanical vibration – Ground-borne noise and vibrations arising from rail systems – Part 1: General guidance. ISO 14837-1:2005.

Lapčík, L., Augustin, P., Píštěk, A. and Bujnoch, L. 2001. Measurement of the dynamic stiffness of recycled rubber based railway track mats according to the DB-TL 918.071 standard. *Applied Acoustics.* Vol. 62, 1123 - 1128.

Lin, T.R., Farag, N.H., Pan, J. 2005. Evaluation of frequency dependent rubber mount stiffness and damping by impact test. *Applied Acoustics.* Vol. 66, 829 - 844.

Lombaert, G., Degrande, G., Kogut, J. and François, S. 2006. The experimental validation of a numerical model for the prediction of railway induced vibrations. *Journal of Sound and Vibration.* Vol. 297, 512 -535.

Lombaert, G., Degrande, G., Vanhauwere, B., Vandeborght, B. and François, S. 2006. The control of ground-borne vibrations from railway traffic by means of continuous floating slabs. *Journal of Sound and Vibration.* Vol. 297, 946 - 961.

Macioce, P. 2003 Viscoelastic damping 101. *Sound and Vibration.* Vol. 37(4), 8 - 10.

Maes, J., Sol, H. and Guillaume, P. 2006. Measurement of the dynamic rail pad properties. *Journal of Sound and Vibration.* Vol. 293, 557 - 565.

Maes, J. and Sol, H. 2003. A double tuned rail damper – increasing damping at the two first pinned-pinned frequencies. *Journal of Sound and Vibration.* Vol. 267, 721 - 737.

Maia, N.M.M., Silva, J.M.M. and Ribeiro, A.M.R. 1998. On a general model for Damping. *Journal of Sound and Vibration.* Vol. 218(5), 749 - 767.

Model 407 Controller Product Manual. 2006. Eden Praire: MTS Systems Corporation.

Nakra, B.C. 1998. Vibration Control in Machines and Structures using Viscoelastic Damping. *Journal of Sound and Vibration.* Vol. 211(3), 449 - 465.

Nielson, J.C.O. and Oscarsson, J. 2004. Simulation of dynamic train-track interaction with state-dependent track properties. *Journal of Sound and Vibration.* Vol. 275, 515 - 532.

Picoux, B. and Le Houédec, D. 2005. Diagnosis and prediction of vibration from railway trains. *Soil Dynamics and Earthquake Engineering.* Vol. 25, 905 - 921.

Remillat, C. 2007. Damping mechanism of polymers filled with elastic particles. *Mechanics of Materials.* Vol. 39, 523 - 537.

Rivin, E.I. 2003. *Passive Vibration Isolation*. New York: ASME Press.

Thompson, D.J., Jones, C.J.C., Waters, T.P. and Farrington, D. 2007. A tuned damping device for reducing noise from railway track. *Applied Acoustics.* Vol. 68, 43 - 57.

Vanderplaats, G.N. 2005. *Numerical Optimization Techniques for Engineering design.* Colorado Springs: Vanderplaats Research & Development Inc.

Vostroukhov, A.V. and Metrikine, A.V. 2003. Periodically supported beam on a viscoelastic layer as a model for dynamic analysis of a high-speed railway track. *International Journal of Solids and Structures.* Vol. 40, 5723 - 5752.

Vriend, N.M. and Kren, A.P. 2004. Determination of the viscoelastic properties of elastomeric materials by the dynamic indentation method. *Polymer Testing.* Vol. 23, 369 - 375.

Woodhouse, J. 1998. Linear Damping models for Structural Vibration. *Journal of Sound and Vibration.* Vol. 215(3), 547 - 569.

Zhai, W. and Cai, Z. 1997. Dynamic interaction between a lumped mass vehicle and a discretely supported continuous rail track. *Computers & Structures.* Vol. 63(5), 987 - 997.

Zhai, W.M., Wang, K.Y. and Lin, J.H. 2004. Modelling and experiment of railway ballast vibrations. *Journal of Sound and Vibration.* Vol. 270, 673 - 683.

Appendix A: Material data sheets

CDM-17 RC

MATERIAL DATA SHEET

MDS_CDM-17-v3 20/11/2007

CDM-RC family: ☐ CDM-15 ■ CDM-17

Load Range [MPa] (*)	Static	Total	Occasional
	0,50 - 1,00	2,00	8,00
E-module [MPa] (*)	Static	Dynamic	
	8,50 - 12,00	25,00 - 40,00	

* with respect to the optimal load range

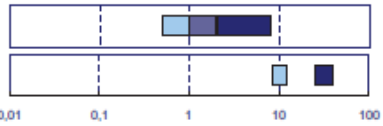

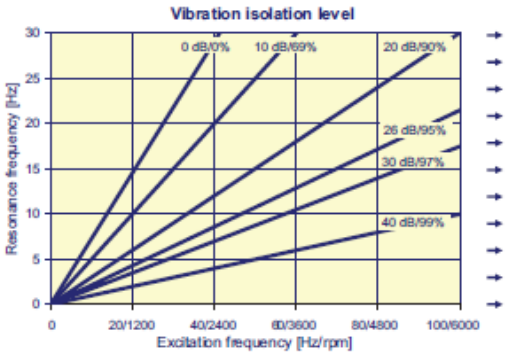

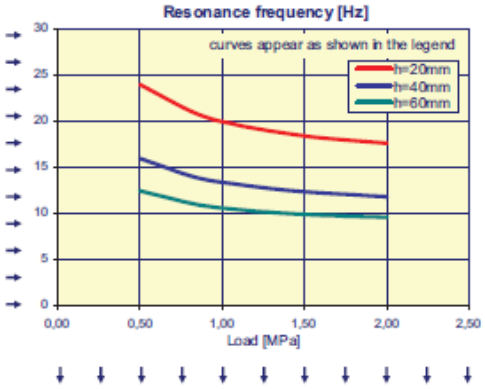

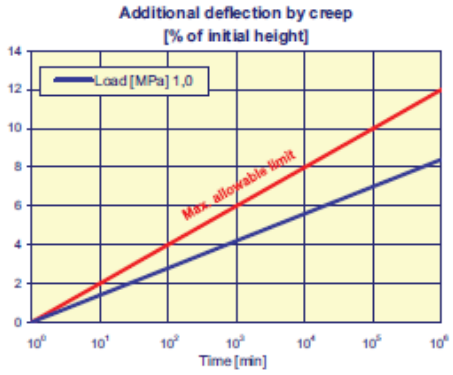

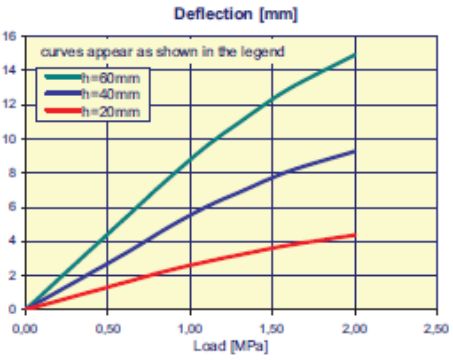

Material	-	R-B Corkelastomer	**Elongation at Break**	ASTM F152	> 50%
Density	-	950 kg/m³	**Compression set 50%/23°C/70h**	DIN 53572	< 8%
Colour	-	Black	**Compressibility at 2.8 MPa**	ASTM F36	10 - 20%
Temperature Range	Constant	-10 / +100°C	**Recovery at 2.8 MPa**	ASTM F36	> 80%
Tensile Strength	ASTM F152	> 1.8 MPa	**Shore hardness**	ASTM D2240	70 - 80 A

These test results are obtained on a sample with a cross section of 60*60mm

CDM
Reutenbeek 9-11
BE - 3090 Overijse
Belgium

noise & vibration control

T: +32-2-687 79 07
F: +32-2-687 35 52
general@cdm.be
www.cdm.be

CDM-45 RR

MATERIAL DATA SHEET

MDS_CDM-45-v4 20/11/2007

CDM-RR family: ☐ CDM-42 ☐ CDM-43 ■ CDM-45 ☐ CDM-46

	Static	Total	Occasional
Load Range [MPa] (*)	0,05 - 0,60	1,60	8,00

	Static	Dynamic
E-module [MPa] (*)	3,00 - 5,00	5,50 - 14,00

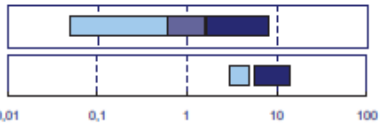

* with respect to the optimal load range

Vibration isolation level

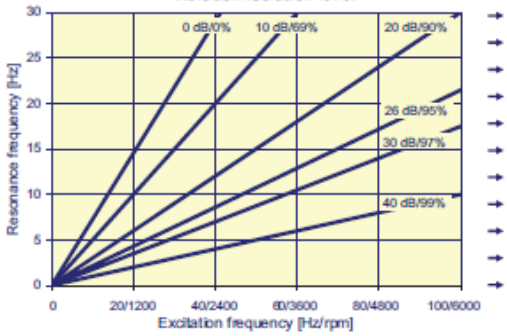

Resonance frequency [Hz]

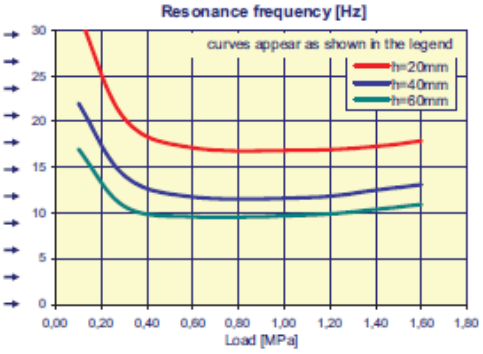

Additional deflection by creep [% of initial height]

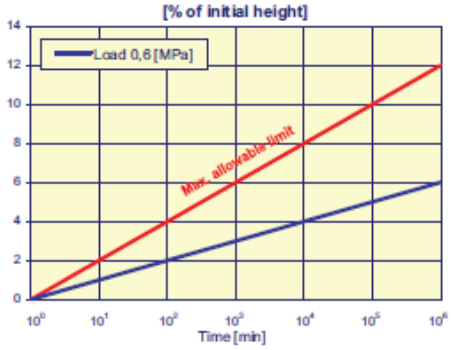

Deflection [mm]

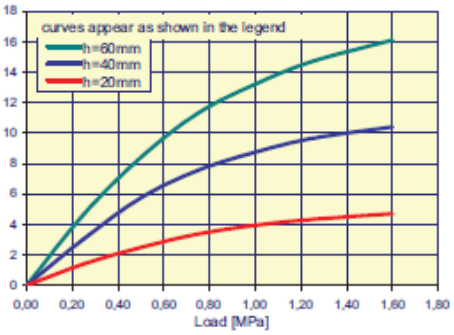

Material	-	Resin Bonded Rubber	**Elongation at Break**	ASTM F152	> 40%
Density	-	810 kg/m³	**Compression set 50%/23°C/70h**	DIN 53572	< 10%
Colour	-	Black	**Compressibility at 2.8 MPa**	ASTM F36	40 - 60%
Temperature Range	Constant	-10 / +100°C	**Recovery at 2.8 MPa**	ASTM F36	> 90%
Tensile Strength	ASTM F152	> 0.5 MPa	**Shore hardness**	ASTM D2240	40 - 50 A

These test results are obtained on a sample with a cross section of 300*300mm

CDM
Reutenbeek 9-11
BE - 3090 Overijse
Belgium

noise & vibration control

T: +32-2-687 79 07
F: +32-2-687 35 52
general@cdm.be
www.cdm.be

CDM-46 RR

MATERIAL DATA SHEET

MDS_CDM-46-v3 20/11/2007

CDM-RR family: ☐ CDM-42 ☐ CDM-43 ☐ CDM-45 ■ CDM-46

Load Range [MPa] (*)	Static	Total	Occasional
	0,10 - 0,90	2,50	10,00
E-module [MPa] (*)	Static	Dynamic	
	4,00 - 8,00	15,00 - 30,00	

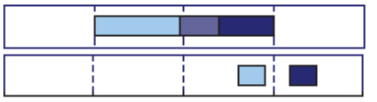

* with respect to the optimal load range

Vibration isolation level

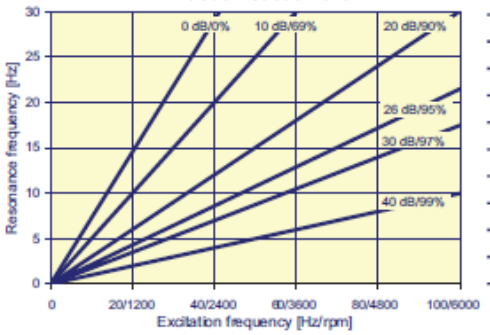

Resonance frequency [Hz]

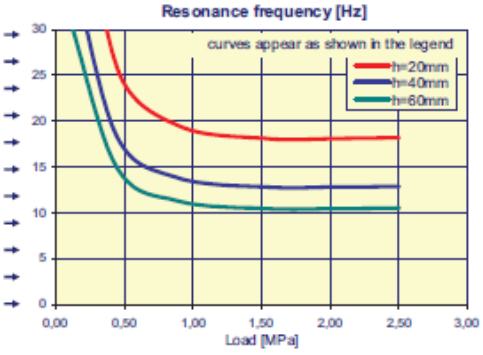

Additional deflection by creep [% of initial height]

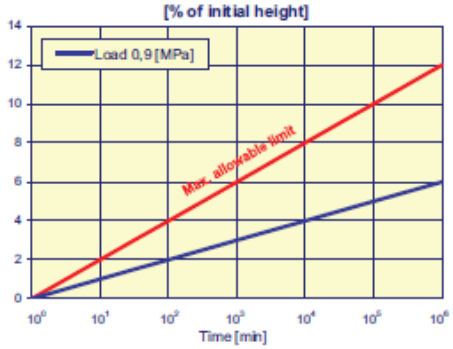

Deflection [mm]

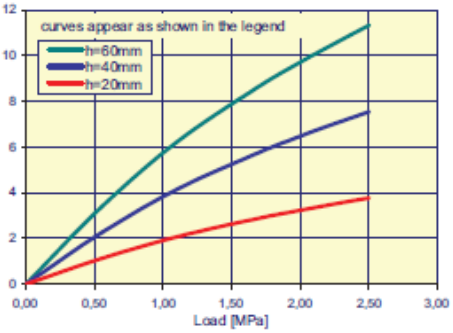

Material	-	Resin Bonded Rubber	**Elongation at Break**	ASTM F152	> 40%
Density	-	990 kg/m³	**Compression set 50%/23°C/70h**	DIN 53572	< 10%
Colour	-	Black	**Compressibility at 2.8 MPa**	ASTM F36	30 - 50%
Temperature Range	Constant	-20 / +140°C	**Recovery at 2.8 MPa**	ASTM F36	> 90%
Tensile Strength	ASTM F152	> 0.5 MPa	**Shore hardness**	ASTM D2240	50 - 60 A

These test results are obtained on a sample with a cross section of 300*300mm

CDM
Reutenbeek 9-11
BE - 3090 Overijse
Belgium

noise & vibration control

T: +32-2-687 79 07
F: +32-2-687 35 52
general@cdm.be
www.cdm.be

Appendix B: Measurement results

Figure B-1: Measurement results for CDM-17 at 4 Hz.

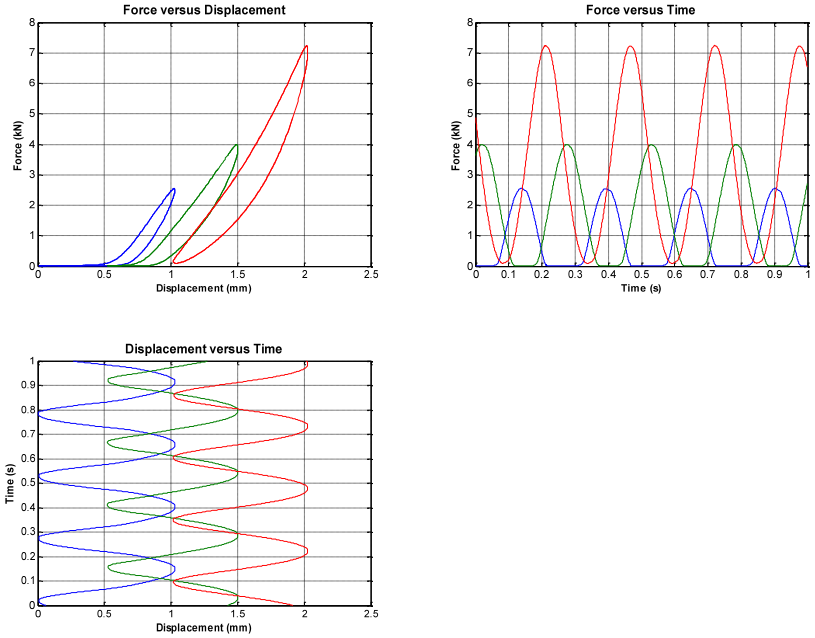

Figure B-2: Measurement results for CDM-17 at 8 Hz.

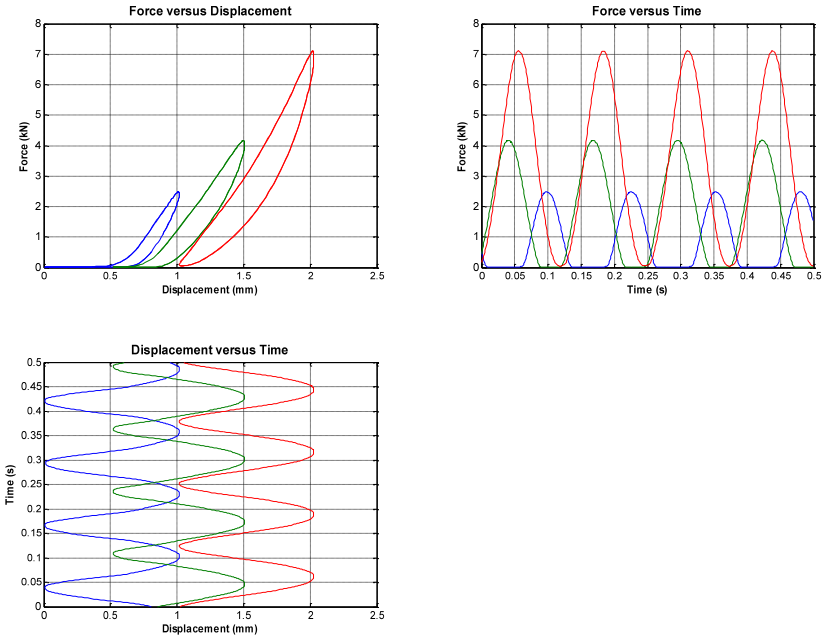

Figure B-3: Measurement results for CDM-17 at 16 Hz.

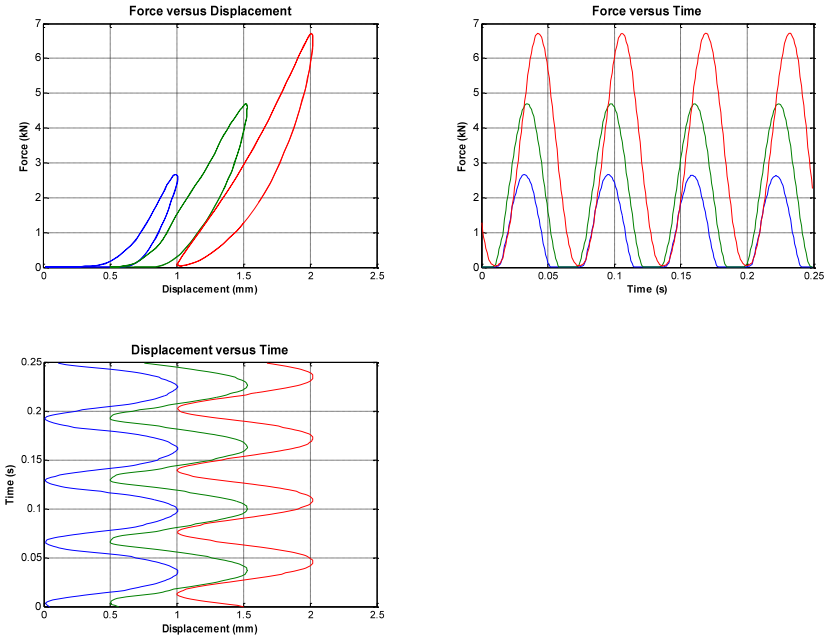

Figure B-4: Measurement results for CDM-45 at 4 Hz

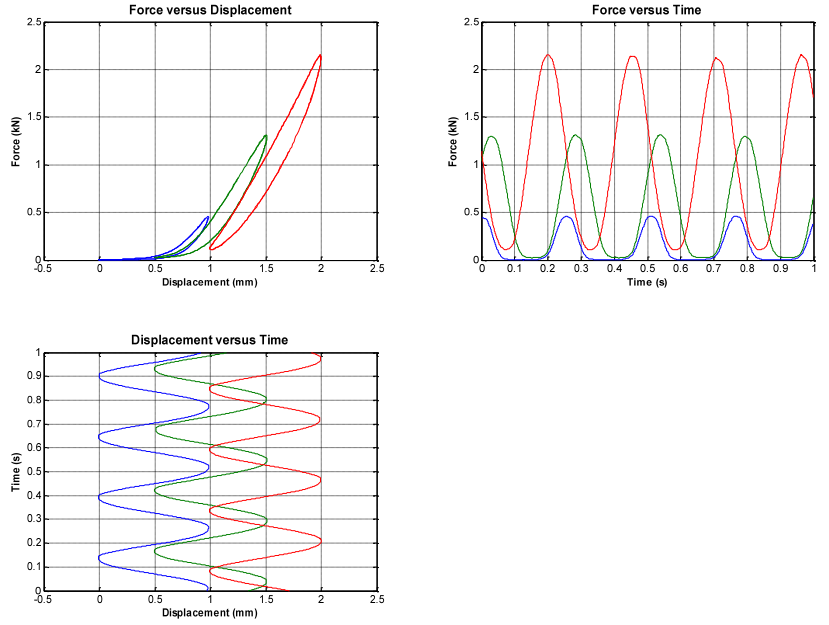

Figure B-5: Measurement results for CDM-45 at 8 Hz.

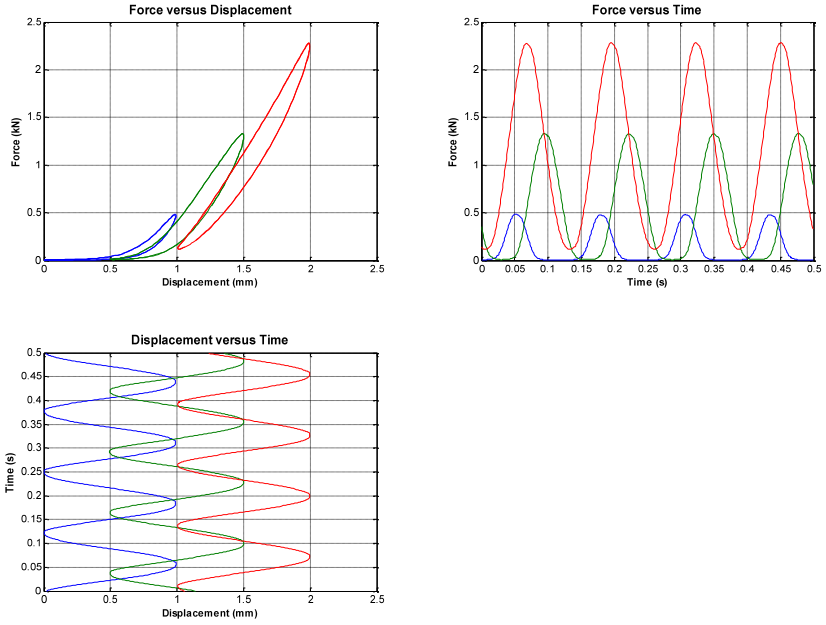

Figure B-6: Measurement results for CDM-45 at 16 Hz.

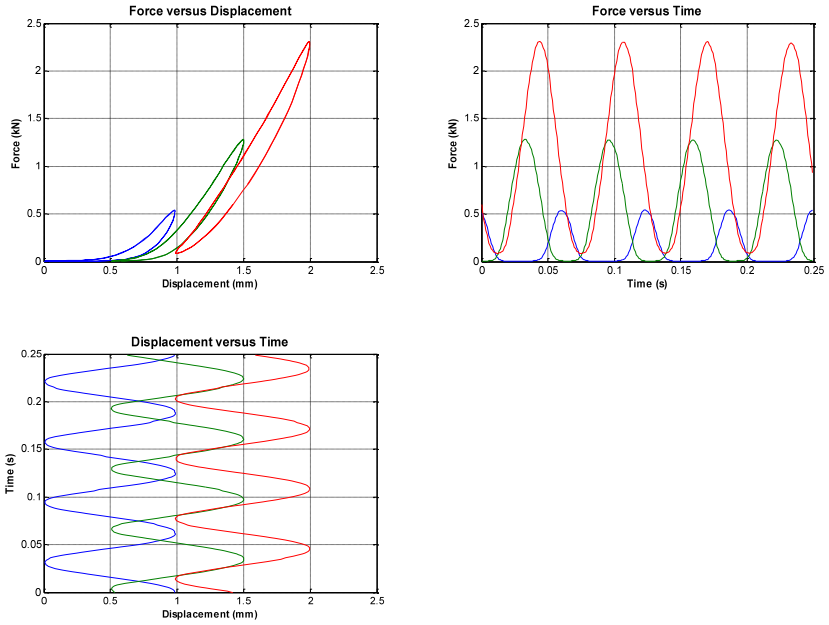

Figure B-7: Measurement results for CDM-46 at 4 Hz.

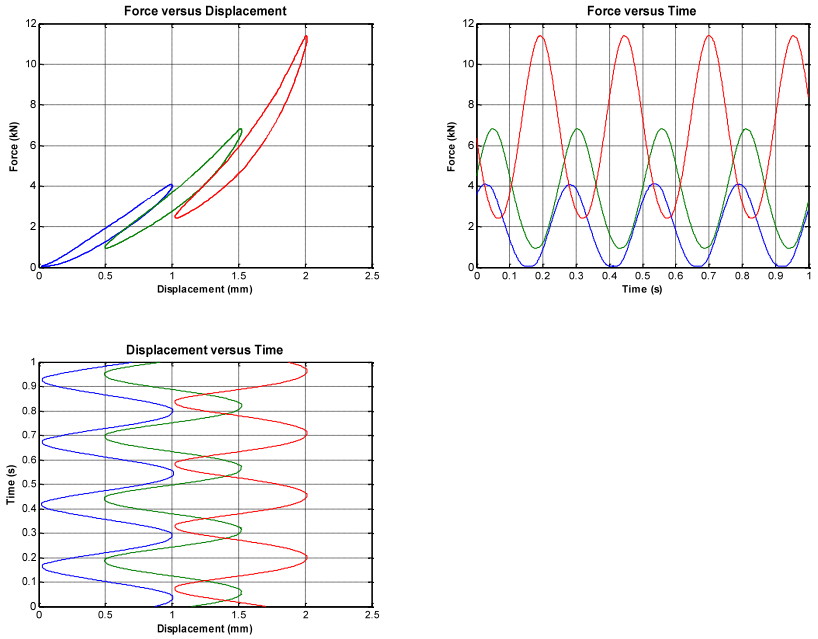

Figure B-8: Measurement results for CDM-46 at 8 Hz.

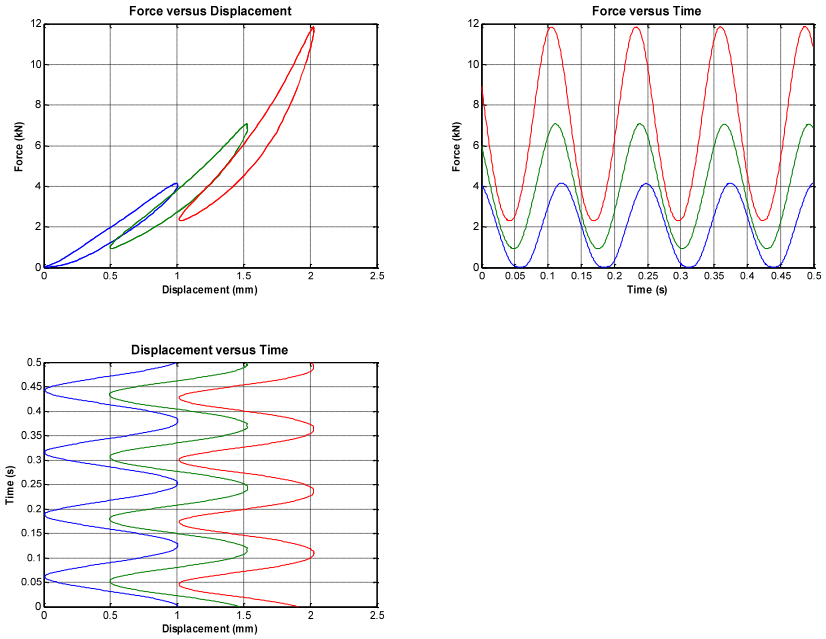

Figure B-9: Measurement results for CDM-46 at 16 Hz.

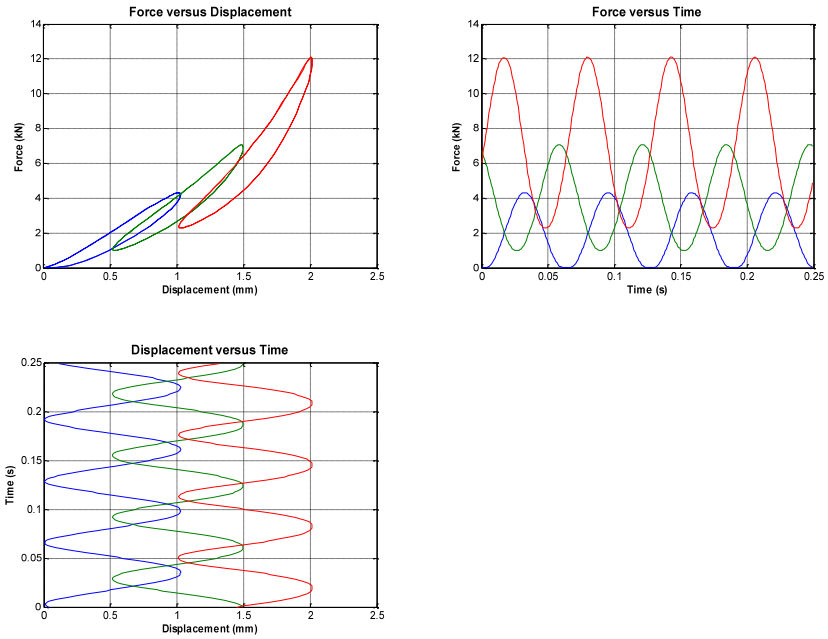

Appendix C: Optimisation results

Table C-1: CDM-17 Individual optimisation coefficients.

	Condition	k_1 [10^{12} N/m^3]	k_2 [10^6 N/m]	k_3 [10^6 N/m]	c [10^6 Ns/m]	Error [10^3]
Non-linear	Preload 1, 4 Hz	2,171	0	n.a.	0,015	7,09
	Preload 1, 8 Hz	2,087	0	n.a.	0,008	9,15
	Preload 1, 16 Hz	2,263	0	n.a.	0,007	7,84
	Preload 2, 4 Hz	1,081	0	n.a.	0,034	5,24
	Preload 2, 8 Hz	1,1	0	n.a.	0,02	5,45
	Preload 2, 16 Hz	1,123	0	n.a.	0,018	2,47
	Preload 3, 4 Hz	0,782	0	n.a.	0,064	3,84
	Preload 3, 8 Hz	0,752	0	n.a.	0,036	3,47
	Preload 3, 16 Hz	0,692	0	n.a.	0,023	1,35
Relaxation	Preload 1, 4 Hz	1,673	0	3,304	0,223	3,35
	Preload 1, 8 Hz	1,58	0	3,85	0,132	1,73
	Preload 1, 16 Hz	1,852	0	4,168	0,058	3,18
	Preload 2, 4 Hz	0,949	0	2,861	0,147	1,04
	Preload 2, 8 Hz	0,979	0	3,182	0,076	1,57
	Preload 2, 16 Hz	0,991	0	3,921	0,041	1,97
	Preload 3, 4 Hz	0,734	0	3,298	0,136	2,89
	Preload 3, 8 Hz	0,705	0	3,564	0,078	2,63
	Preload 3, 16 Hz	0,68	0	3,831	0,036	1,48
Creep	Preload 1, 4 Hz	0,379	0,469	5,35	0,606	0,19
	Preload 1, 8 Hz	0,243	0,18	6,642	0,261	0,23
	Preload 1, 16 Hz	0,088	0,107	7,022	0,089	0,57
	Preload 2, 4 Hz	0,407	0,635	7,192	0,597	0,29
	Preload 2, 8 Hz	0,621	0,205	8,469	0,201	0,27
	Preload 2, 16 Hz	0,211	0,584	8,711	0,108	1,66
	Preload 3, 4 Hz	0,253	1,284	9,303	0,861	0,83
	Preload 3, 8 Hz	0,197	1,135	10,03	0,357	0,94
	Preload 3, 16 Hz	0,674	0,001	27,103	0,029	0,94

Table C-2: CDM-17 Overall optimisation coefficients.

	Condition	k_1 [10^{12} N/m^3]	k_2 [10^6 N/m]	k_3 [10^6 N/m]	c [10^6 Ns/m]	Error [10^3]
Non-linear	Preload 1, 4 Hz	0,661	0,434	n.a.	0,024	76,55
	Preload 1, 8 Hz	0,661	0,434	n.a.	0,024	62,42
	Preload 1, 16 Hz	0,661	0,434	n.a.	0,024	54,97
	Preload 2, 4 Hz	0,661	0,434	n.a.	0,024	20,11
	Preload 2, 8 Hz	0,661	0,434	n.a.	0,024	21,07
	Preload 2, 16 Hz	0,661	0,434	n.a.	0,024	14,32
	Preload 3, 4 Hz	0,661	0,434	n.a.	0,024	11,33
	Preload 3, 8 Hz	0,661	0,434	n.a.	0,024	8,92
	Preload 3, 16 Hz	0,661	0,434	n.a.	0,024	8,51
Relaxation	Preload 1, 4 Hz	0,38	0,917	4,276	0,253	77,33
	Preload 1, 8 Hz	0,38	0,917	4,276	0,253	56,28
	Preload 1, 16 Hz	0,38	0,917	4,276	0,253	23,06
	Preload 2, 4 Hz	0,38	0,917	4,276	0,253	21,55
	Preload 2, 8 Hz	0,38	0,917	4,276	0,253	19,02
	Preload 2, 16 Hz	0,38	0,917	4,276	0,253	3,33
	Preload 3, 4 Hz	0,38	0,917	4,276	0,253	11,24
	Preload 3, 8 Hz	0,38	0,917	4,276	0,253	7,55
	Preload 3, 16 Hz	0,38	0,917	4,276	0,253	12,78
Creep	Preload 1, 4 Hz	0,65	0,473	10,536	0,048	7,01
	Preload 1, 8 Hz	0,65	0,473	10,536	0,048	2,37
	Preload 1, 16 Hz	0,65	0,473	10,536	0,048	5,36
	Preload 2, 4 Hz	0,65	0,473	10,536	0,048	2,43
	Preload 2, 8 Hz	0,65	0,473	10,536	0,048	1,12
	Preload 2, 16 Hz	0,65	0,473	10,536	0,048	7,18
	Preload 3, 4 Hz	0,65	0,473	10,536	0,048	2,4
	Preload 3, 8 Hz	0,65	0,473	10,536	0,048	2,2
	Preload 3, 16 Hz	0,65	0,473	10,536	0,048	7,44

Table C-3: CDM-17 Frequency optimisation coefficients.

	Condition	k_1 [10^{12} N/m^3]	k_2 [10^6 N/m]	k_3 [10^6 N/m]	c [10^6 Ns/m]	Error [10^3]
Non-linear	Preload 1, 4 Hz	0,724	0,34	n.a.	0,046	82,86
	Preload 1, 8 Hz	0,71	0,306	n.a.	0,029	70,53
	Preload 1, 16 Hz	0,557	0,621	n.a.	0,022	51,23
	Preload 2, 4 Hz	0,724	0,34	n.a.	0,046	16,77
	Preload 2, 8 Hz	0,71	0,306	n.a.	0,029	21,03
	Preload 2, 16 Hz	0,557	0,621	n.a.	0,022	17,16
	Preload 3, 4 Hz	0,724	0,34	n.a.	0,046	8,91
	Preload 3, 8 Hz	0,71	0,306	n.a.	0,029	7,44
	Preload 3, 16 Hz	0,557	0,621	n.a.	0,022	5,6
Relaxation	Preload 1, 4 Hz	0,444	0,789	4,162	0,342	3,04
	Preload 1, 8 Hz	0,414	0,816	4,527	0,184	6,72
	Preload 1, 16 Hz	0,277	1,138	5,114	0,103	25,55
	Preload 2, 4 Hz	0,444	0,789	4,162	0,342	2,89
	Preload 2, 8 Hz	0,414	0,816	4,527	0,184	3,08
	Preload 2, 16 Hz	0,277	1,138	5,114	0,103	3,68
	Preload 3, 4 Hz	0,444	0,789	4,162	0,342	2,75
	Preload 3, 8 Hz	0,414	0,816	4,527	0,184	2,62
	Preload 3, 16 Hz	0,277	1,138	5,114	0,103	4,3
Creep	Preload 1, 4 Hz	0,562	0,363	8,926	0,545	2,95
	Preload 1, 8 Hz	0,542	0,151	9,82	0,236	1,94
	Preload 1, 16 Hz	0,467	0,571	10,144	0,061	2,96
	Preload 2, 4 Hz	0,562	0,363	8,926	0,545	0,8
	Preload 2, 8 Hz	0,542	0,151	9,82	0,236	0,6
	Preload 2, 16 Hz	0,467	0,571	10,144	0,061	1,37
	Preload 3, 4 Hz	0,562	0,363	8,926	0,545	1,42
	Preload 3, 8 Hz	0,542	0,151	9,82	0,236	1,49
	Preload 3, 16 Hz	0,467	0,571	10,144	0,061	1,7

Table C-4: CDM-17 Preload optimisation coefficients.

	Condition	k_1 [10^{12} N/m^3]	k_2 [10^6 N/m]	k_3 [10^6 N/m]	c [10^6 Ns/m]	Error [10^3]
Non-linear	Preload 1, 4 Hz	2,166	0,001	n.a.	0,008	7,05
	Preload 1, 8 Hz	2,166	0,001	n.a.	0,008	9,43
	Preload 1, 16 Hz	2,166	0,001	n.a.	0,008	8,11
	Preload 2, 4 Hz	1,099	0,001	n.a.	0,02	6,57
	Preload 2, 8 Hz	1,099	0,001	n.a.	0,02	5,46
	Preload 2, 16 Hz	1,099	0,001	n.a.	0,02	2,6
	Preload 3, 4 Hz	0,743	0,001	n.a.	0,027	6,68
	Preload 3, 8 Hz	0,743	0,001	n.a.	0,027	4,07
	Preload 3, 16 Hz	0,743	0,001	n.a.	0,027	3,62
Relaxation	Preload 1, 4 Hz	1,734	0,001	3,424	0,129	7,13
	Preload 1, 8 Hz	1,734	0,001	3,424	0,129	9,74
	Preload 1, 16 Hz	1,734	0,001	3,424	0,129	8,54
	Preload 2, 4 Hz	1,038	0,001	3,382	0,053	6,5
	Preload 2, 8 Hz	1,038	0,001	3,382	0,053	5,64
	Preload 2, 16 Hz	1,038	0,001	3,382	0,053	2,69
	Preload 3, 4 Hz	0,709	0,001	3,144	0,073	6,73
	Preload 3, 8 Hz	0,709	0,001	3,144	0,073	4,13
	Preload 3, 16 Hz	0,709	0,001	3,144	0,073	3,81
Creep	Preload 1, 4 Hz	2,165	0,001	18,228	0,009	2,3
	Preload 1, 8 Hz	2,165	0,001	18,228	0,009	1,37
	Preload 1, 16 Hz	2,165	0,001	18,228	0,009	4,45
	Preload 2, 4 Hz	1,09	0,001	28,213	0,022	3,27
	Preload 2, 8 Hz	1,09	0,001	28,213	0,022	1,09
	Preload 2, 16 Hz	1,09	0,001	28,213	0,022	1,76
	Preload 3, 4 Hz	0,743	0,001	57,942	0,027	2,91
	Preload 3, 8 Hz	0,743	0,001	57,942	0,027	1,02
	Preload 3, 16 Hz	0,743	0,001	57,942	0,027	5,61

Table C-5: CDM-45 Individual optimisation coefficients.

	Condition	k_1 [10^{12} N/m^3]	k_2 [10^6 N/m]	k_3 [10^6 N/m]	c [10^6 Ns/m]	Error [10^3]
Non-linear	Preload 1, 4 Hz	0,432	0	n.a.	0,002	4,61
	Preload 1, 8 Hz	0,428	0	n.a.	0,002	6,31
	Preload 1, 16 Hz	0,45	0	n.a.	0,002	5,73
	Preload 2, 4 Hz	0,367	0	n.a.	0,008	1,77
	Preload 2, 8 Hz	0,364	0	n.a.	0,006	2,73
	Preload 2, 16 Hz	0,336	0	n.a.	0,003	2,61
	Preload 3, 4 Hz	0,262	0	n.a.	0,015	1,1
	Preload 3, 8 Hz	0,275	0	n.a.	0,008	0,66
	Preload 3, 16 Hz	0,271	0	n.a.	0,005	0,23
Relaxation	Preload 1, 4 Hz	0,307	0	0,613	0,055	5,54
	Preload 1, 8 Hz	0,299	0	0,726	0,027	2,67
	Preload 1, 16 Hz	0,354	0	0,789	0,011	4,27
	Preload 2, 4 Hz	0,33	0,006	0,587	0,029	5,58
	Preload 2, 8 Hz	0,328	0	0,754	0,018	2,98
	Preload 2, 16 Hz	0,303	0	0,76	0,014	1,33
	Preload 3, 4 Hz	0,21	0,122	0,732	0,036	1,64
	Preload 3, 8 Hz	0,221	0,13	0,739	0,02	0,59
	Preload 3, 16 Hz	0,243	0,069	0,708	0,009	0,41
Creep	Preload 1, 4 Hz	0,439	0	1,557	0,002	1,26
	Preload 1, 8 Hz	0,132	0	1,248	0,033	1,48
	Preload 1, 16 Hz	0,038	0,028	1,385	0,014	1,32
	Preload 2, 4 Hz	0,368	0	19,353	0,008	0,5
	Preload 2, 8 Hz	0,362	0	5,664	0,007	0,41
	Preload 2, 16 Hz	0,183	0	2,58	0,022	0,34
	Preload 3, 4 Hz	0,168	0,302	2,43	0,149	0,18
	Preload 3, 8 Hz	0,273	0	5,518	0,012	0,15
	Preload 3, 16 Hz	0,27	0	8,899	0,005	0,18

Table C-6: CDM-45 Overall optimisation coefficients.

	Condition	k_1 [10^{12} N/m^3]	k_2 [10^6 N/m]	k_3 [10^6 N/m]	c [10^6 Ns/m]	Error [10^3]
Non-linear	Preload 1, 4 Hz	0,266	0,048	n.a.	0,005	16,7
	Preload 1, 8 Hz	0,266	0,048	n.a.	0,005	24,83
	Preload 1, 16 Hz	0,266	0,048	n.a.	0,005	25,44
	Preload 2, 4 Hz	0,266	0,048	n.a.	0,005	15,87
	Preload 2, 8 Hz	0,266	0,048	n.a.	0,005	14,54
	Preload 2, 16 Hz	0,266	0,048	n.a.	0,005	7,14
	Preload 3, 4 Hz	0,266	0,048	n.a.	0,005	5,01
	Preload 3, 8 Hz	0,266	0,048	n.a.	0,005	1,89
	Preload 3, 16 Hz	0,266	0,048	n.a.	0,005	0,86
Relaxation	Preload 1, 4 Hz	0,271	0	0	0,008	19,09
	Preload 1, 8 Hz	0,271	0	0	0,008	31,44
	Preload 1, 16 Hz	0,271	0	0	0,008	32,29
	Preload 2, 4 Hz	0,271	0	0	0,008	16,3
	Preload 2, 8 Hz	0,271	0	0	0,008	13,51
	Preload 2, 16 Hz	0,271	0	0	0,008	4,15
	Preload 3, 4 Hz	0,271	0	0	0,008	4,38
	Preload 3, 8 Hz	0,271	0	0	0,008	1,76
	Preload 3, 16 Hz	0,271	0	0	0,008	1,79
Creep	Preload 1, 4 Hz	0,269	0,043	3,862	0,008	201,45
	Preload 1, 8 Hz	0,269	0,043	3,862	0,008	36,22
	Preload 1, 16 Hz	0,269	0,043	3,862	0,008	53,52
	Preload 2, 4 Hz	0,269	0,043	3,862	0,008	25,33
	Preload 2, 8 Hz	0,269	0,043	3,862	0,008	28,05
	Preload 2, 16 Hz	0,269	0,043	3,862	0,008	22,21
	Preload 3, 4 Hz	0,269	0,043	3,862	0,008	5,32
	Preload 3, 8 Hz	0,269	0,043	3,862	0,008	4,75
	Preload 3, 16 Hz	0,269	0,043	3,862	0,008	5,4

Table C-7: CDM-45 Frequency optimisation coefficients.

	Condition	k_1 [10^{12} N/m^3]	k_2 [10^6 N/m]	k_3 [10^6 N/m]	c [10^6 Ns/m]	Error [10^3]
Non-linear	Preload 1, 4 Hz	0,254	0,068	n.a.	0,01	23,74
	Preload 1, 8 Hz	0,274	0,04	n.a.	0,007	34,36
	Preload 1, 16 Hz	0,27	0,028	n.a.	0,004	20,09
	Preload 2, 4 Hz	0,254	0,068	n.a.	0,01	16,09
	Preload 2, 8 Hz	0,274	0,04	n.a.	0,007	12,59
	Preload 2, 16 Hz	0,27	0,028	n.a.	0,004	7,77
	Preload 3, 4 Hz	0,254	0,068	n.a.	0,01	3,43
	Preload 3, 8 Hz	0,274	0,04	n.a.	0,007	1,7
	Preload 3, 16 Hz	0,27	0,028	n.a.	0,004	0,65
Relaxation	Preload 1, 4 Hz	0,205	0,142	0,713	0,048	76,03
	Preload 1, 8 Hz	0,228	0,115	0,739	0,023	76,11
	Preload 1, 16 Hz	0,225	0,109	0,799	0,015	47,85
	Preload 2, 4 Hz	0,205	0,142	0,713	0,048	141,29
	Preload 2, 8 Hz	0,228	0,115	0,739	0,023	135,57
	Preload 2, 16 Hz	0,225	0,109	0,799	0,015	153,21
	Preload 3, 4 Hz	0,205	0,142	0,713	0,048	157,56
	Preload 3, 8 Hz	0,228	0,115	0,739	0,023	240,47
	Preload 3, 16 Hz	0,225	0,109	0,799	0,015	219,83
Creep	Preload 1, 4 Hz	0,01	0,02	2,446	0,054	16,89
	Preload 1, 8 Hz	0,014	0,011	2,586	0,019	14,75
	Preload 1, 16 Hz	0,018	0,021	3,585	0,008	3,56
	Preload 2, 4 Hz	0,054	0,02	2,446	0,054	3,68
	Preload 2, 8 Hz	0,049	0,011	2,586	0,019	2,7
	Preload 2, 16 Hz	0,014	0,021	3,585	0,008	1,22
	Preload 3, 4 Hz	0,039	0,02	2,446	0,054	0,39
	Preload 3, 8 Hz	0,018	0,011	2,586	0,019	0,31
	Preload 3, 16 Hz	0,018	0,021	3,585	0,008	0,56

Table C-8: CDM-45 Preload optimisation coefficients.

	Condition	k_1 [10^{12} N/m^3]	k_2 [10^6 N/m]	k_3 [10^6 N/m]	c [10^6 Ns/m]	Error [10^3]
Non-linear	Preload 1, 4 Hz	0,436	0	n.a.	0,002	4,67
	Preload 1, 8 Hz	0,436	0	n.a.	0,002	6,46
	Preload 1, 16 Hz	0,436	0	n.a.	0,002	5,68
	Preload 2, 4 Hz	0,356	0	n.a.	0,004	2,99
	Preload 2, 8 Hz	0,356	0	n.a.	0,004	3,32
	Preload 2, 16 Hz	0,356	0	n.a.	0,004	4,26
	Preload 3, 4 Hz	0,269	0	n.a.	0,006	2,72
	Preload 3, 8 Hz	0,269	0	n.a.	0,006	1,11
	Preload 3, 16 Hz	0,269	0	n.a.	0,006	0,57
Relaxation	Preload 1, 4 Hz	0,334	0	0,61	0,024	10,96
	Preload 1, 8 Hz	0,334	0	0,61	0,024	11,54
	Preload 1, 16 Hz	0,334	0	0,61	0,024	14,39
	Preload 2, 4 Hz	0,323	0	0,656	0,021	3,98
	Preload 2, 8 Hz	0,323	0	0,656	0,021	4,04
	Preload 2, 16 Hz	0,323	0	0,656	0,021	6,27
	Preload 3, 4 Hz	0,229	0,094	0,715	0,019	2,45
	Preload 3, 8 Hz	0,229	0,094	0,715	0,019	1,05
	Preload 3, 16 Hz	0,229	0,094	0,715	0,019	1,16
Creep	Preload 1, 4 Hz	0,347	0	1,221	0,008	3,06
	Preload 1, 8 Hz	0,347	0	1,221	0,008	2,22
	Preload 1, 16 Hz	0,347	0	1,221	0,008	4,81
	Preload 2, 4 Hz	0,343	0	3,336	0,008	1,62
	Preload 2, 8 Hz	0,343	0	3,336	0,008	0,7
	Preload 2, 16 Hz	0,343	0	3,336	0,008	1,9
	Preload 3, 4 Hz	0,267	0	6,802	0,008	0,92
	Preload 3, 8 Hz	0,267	0	6,802	0,008	0,23
	Preload 3, 16 Hz	0,267	0	6,802	0,008	0,94

Table C-9: CDM-46 Individual optimisation coefficients.

	Condition	k_1 [10^{12} N/m^3]	k_2 [10^6 N/m]	k_3 [10^6 N/m]	c [10^6 Ns/m]	Error [10^3]
Non-linear	Preload 1, 4 Hz	1,182	2,828	n.a.	0,028	0,32
	Preload 1, 8 Hz	1,102	2,879	n.a.	0,017	0,34
	Preload 1, 16 Hz	0,798	2,951	n.a.	0,013	0,51
	Preload 2, 4 Hz	0,957	2,172	n.a.	0,037	0,25
	Preload 2, 8 Hz	0,918	2,29	n.a.	0,023	0,26
	Preload 2, 16 Hz	0,672	2,767	n.a.	0,017	0,34
	Preload 3, 4 Hz	1,033	1,269	n.a.	0,052	0,44
	Preload 3, 8 Hz	1,028	1,321	n.a.	0,031	0,68
	Preload 3, 16 Hz	0,898	1,827	n.a.	0,022	0,97
Relaxation	Preload 1, 4 Hz	0,837	2,986	1,543	0,04	0,33
	Preload 1, 8 Hz	0,812	3,015	1,82	0,024	9,98
	Preload 1, 16 Hz	0,588	3,101	2,333	0,019	0,7
	Preload 2, 4 Hz	0,771	2,436	2,054	0,051	0,26
	Preload 2, 8 Hz	0,814	2,442	2,645	0,029	128,99
	Preload 2, 16 Hz	0,775	2,624	3,447	0,02	0,54
	Preload 3, 4 Hz	1,046	1,232	13,658	0,057	902,18
	Preload 3, 8 Hz	1,069	1,207	9,41	0,035	0,72
	Preload 3, 16 Hz	1,026	1,464	6,04	0,023	388,63
Creep	Preload 1, 4 Hz	1,236	2,958	64,189	0,029	0,14
	Preload 1, 8 Hz	1,048	1,054	5,214	0,667	0,18
	Preload 1, 16 Hz	0,841	3,313	28,672	0,016	0,37
	Preload 2, 4 Hz	0,981	2,227	88,896	0,038	0,17
	Preload 2, 8 Hz	0,955	2,394	55,287	0,024	0,24
	Preload 2, 16 Hz	0,708	2,979	42,192	0,019	0,33
	Preload 3, 4 Hz	1,043	1,283	124,257	0,052	0,43
	Preload 3, 8 Hz	1,046	1,347	74,492	0,032	0,61
	Preload 3, 16 Hz	0,924	1,907	53,999	0,023	0,82

Table C-10: CDM-46 Overall optimisation coefficients.

	Condition	k_1 [10^{12} N/m^3]	k_2 [10^6 N/m]	k_3 [10^6 N/m]	c [10^6 Ns/m]	Error [10^3]
Non-linear	Preload 1, 4 Hz	0,705	2,491	n.a.	0,025	12,17
	Preload 1, 8 Hz	0,705	2,491	n.a.	0,025	11,18
	Preload 1, 16 Hz	0,705	2,491	n.a.	0,025	6,24
	Preload 2, 4 Hz	0,705	2,491	n.a.	0,025	1,65
	Preload 2, 8 Hz	0,705	2,491	n.a.	0,025	1,29
	Preload 2, 16 Hz	0,705	2,491	n.a.	0,025	2,59
	Preload 3, 4 Hz	0,705	2,491	n.a.	0,025	3,95
	Preload 3, 8 Hz	0,705	2,491	n.a.	0,025	3,4
	Preload 3, 16 Hz	0,705	2,491	n.a.	0,025	1,6
Relaxation	Preload 1, 4 Hz	0,623	2,631	2,664	0,057	11,91
	Preload 1, 8 Hz	0,623	2,631	2,664	0,057	10,75
	Preload 1, 16 Hz	0,623	2,631	2,664	0,057	5,62
	Preload 2, 4 Hz	0,623	2,631	2,664	0,057	1,69
	Preload 2, 8 Hz	0,623	2,631	2,664	0,057	1,29
	Preload 2, 16 Hz	0,623	2,631	2,664	0,057	2,81
	Preload 3, 4 Hz	0,623	2,631	2,664	0,057	3,99
	Preload 3, 8 Hz	0,623	2,631	2,664	0,057	3,47
	Preload 3, 16 Hz	0,623	2,631	2,664	0,057	1,77
Creep	Preload 1, 4 Hz	0,749	2,675	38,267	0,028	7,07
	Preload 1, 8 Hz	0,749	2,675	38,267	0,028	4,26
	Preload 1, 16 Hz	0,749	2,675	38,267	0,028	4,71
	Preload 2, 4 Hz	0,749	2,675	38,267	0,028	0,55
	Preload 2, 8 Hz	0,749	2,675	38,267	0,028	1,14
	Preload 2, 16 Hz	0,749	2,675	38,267	0,028	4,01
	Preload 3, 4 Hz	0,749	2,675	38,267	0,028	2,84
	Preload 3, 8 Hz	0,749	2,675	38,267	0,028	1,77
	Preload 3, 16 Hz	0,749	2,675	38,267	0,028	1,91

Table C-11: CDM-46 Frequency optimisation coefficients.

	Condition	k_1 [10^{12} N/m^3]	k_2 [10^6 N/m]	k_3 [10^6 N/m]	c [10^6 Ns/m]	Error [10^3]
Non-linear	Preload 1, 4 Hz	0,71	2,433	n.a.	0,044	15,2
	Preload 1, 8 Hz	0,718	2,461	n.a.	0,029	12,32
	Preload 1, 16 Hz	0,685	2,589	n.a.	0,022	4,35
	Preload 2, 4 Hz	0,71	2,433	n.a.	0,044	1,58
	Preload 2, 8 Hz	0,718	2,461	n.a.	0,029	1,38
	Preload 2, 16 Hz	0,685	2,589	n.a.	0,022	1,27
	Preload 3, 4 Hz	0,71	2,433	n.a.	0,044	3,13
	Preload 3, 8 Hz	0,718	2,461	n.a.	0,029	3,11
	Preload 3, 16 Hz	0,685	2,589	n.a.	0,022	1,98
Relaxation	Preload 1, 4 Hz	0,583	2,631	2,151	0,125	14,5
	Preload 1, 8 Hz	0,602	2,644	2,544	0,067	10,53
	Preload 1, 16 Hz	0,633	2,687	3,191	0,034	4,2
	Preload 2, 4 Hz	0,583	2,631	2,151	0,125	1,38
	Preload 2, 8 Hz	0,602	2,644	2,544	0,067	1,52
	Preload 2, 16 Hz	0,633	2,687	3,191	0,034	1,48
	Preload 3, 4 Hz	0,583	2,631	2,151	0,125	3,11
	Preload 3, 8 Hz	0,602	2,644	2,544	0,067	3,05
	Preload 3, 16 Hz	0,633	2,687	3,191	0,034	2,15
Creep	Preload 1, 4 Hz	0,807	2,79	20,041	0,07	3,89
	Preload 1, 8 Hz	0,814	2,905	17,95	0,051	3,87
	Preload 1, 16 Hz	0,723	2,768	42,452	0,024	2,77
	Preload 2, 4 Hz	0,807	2,79	20,041	0,07	1,08
	Preload 2, 8 Hz	0,814	2,905	17,95	0,051	1,5
	Preload 2, 16 Hz	0,723	2,768	42,452	0,024	1,5
	Preload 3, 4 Hz	0,807	2,79	20,041	0,07	1,29
	Preload 3, 8 Hz	0,814	2,905	17,95	0,051	1,59
	Preload 3, 16 Hz	0,723	2,768	42,452	0,024	1,68

Table C-12: CDM-46 Preload optimisation coefficients.

	Condition	k_1 [10^{12} N/m^3]	k_2 [10^6 N/m]	k_3 [10^6 N/m]	c [10^6 Ns/m]	Error [10^3]
Non-linear	Preload 1, 4 Hz	1,019	2,89	n.a.	0,014	1,22
	Preload 1, 8 Hz	1,019	2,89	n.a.	0,014	0,57
	Preload 1, 16 Hz	1,019	2,89	n.a.	0,014	0,94
	Preload 2, 4 Hz	0,867	2,382	n.a.	0,019	1,14
	Preload 2, 8 Hz	0,867	2,382	n.a.	0,019	0,41
	Preload 2, 16 Hz	0,867	2,382	n.a.	0,019	0,94
	Preload 3, 4 Hz	0,991	1,46	n.a.	0,024	0,9
	Preload 3, 8 Hz	0,991	1,46	n.a.	0,024	0,82
	Preload 3, 16 Hz	0,991	1,46	n.a.	0,024	1,29
Relaxation	Preload 1, 4 Hz	0,926	2,954	2,42	0,019	1,25
	Preload 1, 8 Hz	0,926	2,954	2,42	0,019	0,64
	Preload 1, 16 Hz	0,926	2,954	2,42	0,019	1,21
	Preload 2, 4 Hz	0,876	2,372	3,442	0,022	1,17
	Preload 2, 8 Hz	0,876	2,372	3,442	0,022	0,47
	Preload 2, 16 Hz	0,876	2,372	3,442	0,022	1,13
	Preload 3, 4 Hz	1,023	1,37	5,574	0,028	732,72
	Preload 3, 8 Hz	1,023	1,37	5,574	0,028	276,42
	Preload 3, 16 Hz	1,023	1,37	5,574	0,028	105,91
Creep	Preload 1, 4 Hz	1,105	3,193	31,204	0,016	0,92
	Preload 1, 8 Hz	1,105	3,193	31,204	0,016	0,32
	Preload 1, 16 Hz	1,105	3,193	31,204	0,016	0,88
	Preload 2, 4 Hz	0,912	2,521	44,963	0,02	1,04
	Preload 2, 8 Hz	0,912	2,521	44,963	0,02	0,36
	Preload 2, 16 Hz	0,912	2,521	44,963	0,02	0,75
	Preload 3, 4 Hz	1,015	1,502	58,61	0,025	0,82
	Preload 3, 8 Hz	1,015	1,502	58,61	0,025	0,71
	Preload 3, 16 Hz	1,015	1,502	58,61	0,025	1,1